

# A discrete cell model with adaptive signalling for aggregation of *Dictyostelium discoideum*

JOHN C. DALLON AND HANS G. OTHMER

*Department of Mathematics, University of Utah, Salt Lake City, UT 84112, USA*

## CONTENTS

	PAGE
1. Introduction	391
2. The mathematical model	393
(a) Signal transduction	393
(b) Movement rules	395
3. Results from simulations of the model	397
(a) Experiments with different movement rules	397
(b) The effects of AC activity on patterns of aggregation	401
(c) The effects of density on aggregation patterns	402
(d) Formation of spiral waves	407
(e) Simulations with many pacemakers	409
(f) Direction selection	410
4. Conclusions	411
Appendix 1. Cell weights	413
Appendix 2. The numerical methods and their implementation	414
Appendix 3. Random variables	416
References	416

## SUMMARY

*Dictyostelium discoideum* (Dd) is a widely studied model system from which fundamental insights into cell movement, chemotaxis, aggregation and pattern formation can be gained. In this system aggregation results from the chemotactic response by dispersed amoebae to a travelling wave of the chemoattractant cAMP. We have developed a model in which the cells are treated as discrete points in a continuum field of the chemoattractant, and transduction of the extracellular cAMP signal into the intracellular signal is based on the G protein model developed by Tang & Othmer. The model reproduces a number of experimental observations and gives further insight into the aggregation process. We investigate different rules for cell movement, the factors that influence stream formation, the effect on aggregation of noise in the choice of the direction of movement, and when spiral waves of chemoattractant and cell density are likely to occur. Our results give new insight into the origin of spiral waves and suggest that streaming is due to a finite amplitude instability.

## 1. INTRODUCTION

*Dictyostelium discoideum* (Dd) is a widely studied system because its life cycle incorporates a number of basic processes that occur throughout developmental biology. Dd cells live as individual amoebae during the vegetative cycle of their life, feed on decaying logs, humus and bacteria (Bonner 1982), and multiply by binary fission. After a period of starvation they become chemotactically sensitive to cyclic adenosine 3',5'-monophosphate (cAMP), as well as relay competent. As a result, the cells sense and move toward a source of cAMP, and they relay the signal as well by secreting cAMP. Virtually all of the cells are relay competent 6–10 h after the onset of starvation (Gingle & Robertson 1976). After about 8 h

of starvation randomly located cells, called pacemakers, begin to emit cAMP periodically (Raman *et al.* 1976), the chemotactically competent cells move toward these pacemakers, and eventually the entire population forms a mound-shaped aggregate of up to  $10^5$  cells. Differentiation into anterior and posterior cells begins in the mound stage. Usually the mound topples over and forms a slug, and after migrating for a period of time, the slug forms a fruiting body. The anterior cells push down through the posterior cells, thereby forming a stalk tube, and the posterior cells migrate upward along this tube. The posterior cells become spores which remain dormant until conditions are favourable, at which time the life cycle begins again.

A great deal has been learned about signal trans-

duction, gene control and pattern formation in Dd, and there are mathematical models for a number of these processes (Tang & Othmer 1994; Schaap *et al.* 1997). However, there are a number of basic questions about cell movement in aggregation and in the slug that are unresolved, including the microscopic issues of how a cell decides when to move, how it determines the direction in which to move, and how long it moves. Since cell movement plays a fundamental role in such diverse processes as embryonic development, the response of the immune system, and wound healing, a better understanding of cell movement in Dd will be valuable in a number of other contexts. Knowledge of the behaviour of individual cells will also help in understanding the types of collective cell motion possible in populations of cells, including the various types of aggregation patterns seen in Dd. In this paper we develop and analyse a discrete cell model for the aggregation of Dd that incorporates a realistic model for signal transduction, cAMP production and cAMP release, and which allows us to explore the effect on macroscopic aggregation patterns of changes in the microscopic rules by which cells determine their direction and duration of movement. Our objectives are to understand (a) whether cell motion is determined by the local temporal or spatial gradient of cAMP, or neither, (b) what properties of the cells and their initial distribution in space determines whether spirals or target patterns form in aggregation, (c) what factors determine whether streams are formed in aggregation, and (d) how the fraction of pacemakers affects the size and morphology of the aggregation territories. The model we develop is sufficiently robust that we can study the effect of experimental alterations of properties, such as excitability, on the aggregation patterns, and we can compare the predicted behaviour for various mutants with the observed aggregation patterns.

Earlier models of Dd aggregation can be grouped into two major categories: those that treat the cells as discrete units and those which use a continuum description for the cell density. Although these models have given some insight into the aggregation process, they all have limitations which preclude a detailed analysis of the questions we address. The models developed by Parnas & Segel (1977), MacKay (1978) and Vasieva *et al.* (1994) fall into the first category. The first two of these are similar in that in each the cells are treated as black boxes which, when stimulated, output a fixed amount of cAMP. No description of signal transduction, cAMP production, or adaptation is incorporated, but diffusion of cAMP is taken into account. The model of Parnas & Segel only deals with one space dimension and can only address the questions of how the cell decides when to move and, in a very simplistic manner, which direction the cell moves. MacKay's model is two dimensional and can reproduce the observed streaming patterns, the effect of two competing pacemakers, and spiral waves. These models are a first step in the modelling process, but the rules are formal and

not based on a mechanistic description of signal detection, transduction, cAMP production, and cAMP secretion. In more recent modelling by Vasieva *et al.* the diffusion of cAMP is not even incorporated; instead they use a cellular automaton model with rules by which neighbours are activated. They are able to reproduce streaming patterns and find self-sustaining sources of excitation, but because the model is purely formal, little can be said about its relevance to Dd aggregation.

The models developed by Levine & Reynolds (1991), Vasiev *et al.* (1994) and Höfer *et al.* (1995) fall into the second category. The Levine & Reynolds and Höfer *et al.* models are based on a modified form of the Martiel & Goldbeter (1984) model for cAMP production and signalling, whereas Vasiev *et al.* use a modified FitzHugh–Nagumo model for these processes. Several objections can be raised to either of the models for the local dynamics. First, the Martiel & Goldbeter (1984) model is based on receptor desensitization by phosphorylation as the mechanism for adaptation, but it is now known that this is not how adaptation occurs. A more serious objection is that there is no single Martiel & Goldbeter (1984) model that describes the different behaviours in Dd; the parameters which describe the behaviour in suspensions must be changed by orders of magnitude to reproduce the observed waves (Tyson *et al.* 1989), and there is no suggestion in the literature that such changes are realistic. The FitzHugh–Nagumo model is even less suitable as a model for the local dynamics, for it incorporates nothing of what is known about signal transduction and cAMP production in Dd. Furthermore, since Höfer *et al.* and Levine & Reynolds use continuum chemotaxis equations to describe cell motion, *ad hoc* assumptions are needed to incorporate adaptation of the tactic component of the movement. The need for such assumptions can be understood as follows. Adaptation in the signal transduction system leads to adaptation in the locomotory response, which means that there is no bias in the random movement when there is no spatial or temporal variation of extracellular cAMP. Thus it is the intracellular dynamics which determine the tactic component of the motion, and at present there is no algorithm or procedure for translating the 'rules' for individual cell motion into macroscopic parameters such as the chemotactic sensitivity when the sensory systems adapt. In fact work on this problem suggests that the intracellular dynamics must be retained for an adequate description of motion in the presence of adaptation (Othmer 1997).

The attraction of continuum models is that it is somewhat easier to obtain analytical insights from continuum descriptions with simplified local dynamics, and the computational algorithms needed to simulate the evolution are relatively simple. The primary insights gained from these models relate to the apparent instabilities which cause streaming patterns. Vasiev *et al.* conclude that the major factor in stream formation is a change in the speed of the cAMP wave

as density varies, but we do not agree with that conclusion. Levine & Reynolds conclude that stream formation is the result of an instability generated by the coupling of the density and the signalling. Höfer *et al.* conclude that patterns are generated by an interaction of the excitable medium and the multicellular morphogenesis.

Despite the analytical and computational simplicity of continuum models, we have developed a hybrid discrete/continuum model in which the cells are treated as individual units and the extracellular cAMP is described by a continuum reaction-diffusion equation. A detailed description of signal transduction and adaptation is possible in such a model, and movement rules based on the intracellular dynamics can be explored. We use the Tang & Othmer (1994) signal transduction model, which incorporates the known biology more completely than any other model. In addition, it also produces the correct cAMP levels in both the perfusion and suspension experiments without a change of parameters (Tang & Othmer 1994), and predicts the observed wave speeds and spatial patterns of cAMP when the cells are immobile (Tang & Othmer 1995). Not only does this model allow us to examine in detail how changes in the microscopic rules for movement affect the macroscopic patterns of aggregation, but by comparing the results of our model with the results of the previous models we can determine which predictions are model dependent and which are likely to be biologically significant.

In the following section we describe the model, which is done in two steps. First, we describe the cAMP production and diffusion component, and indicate how the resulting equations are solved numerically. Following this we introduce two sets of movement rules and provide the justification for their use. In § 3 we present the results of the numerical simulations, which address five issues. First, we discuss simulations with various movement rules, and then we present numerical results that simulate experiments in which the excitability of the system is modified. Next we study the effect of density on the observed patterns of aggregation and we explore the effect of varying the fraction of pacemakers on the aggregation patterns. Finally, we look at the sensitivity of the system to the cell's chosen direction. We conclude with a discussion of the insights that are gained from this model.

## 2. THE MATHEMATICAL MODEL

### (a) Signal transduction

The mathematical model developed in Tang & Othmer (1994) and Tang & Othmer (1995) postulates two major pathways in the transduction of and adaptation to an extracellular cAMP signal. cAMP (denoted H) binds to the receptors cAR1 (denoted  $R_s$ ), and the complex  $HR_s$  catalyses the activation of the  $\alpha$  subunit  $G'_s$  of the stimulatory G protein  $G_s$ . This in turn binds with the inactive form of adenylyl cyclase (AC) and produces the activated form  $G'_sAC$ .

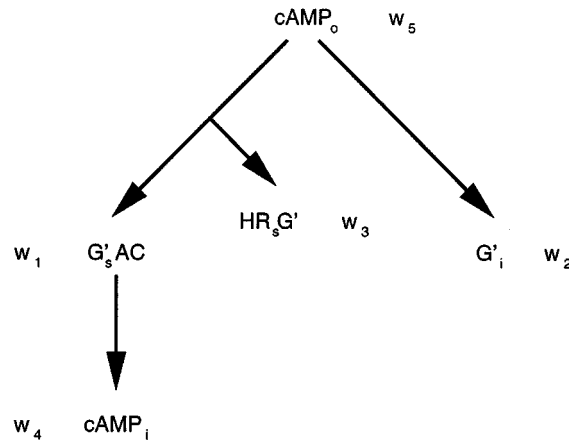


Figure 1. A schematic of the simplified transduction and adaptation scheme in Tang & Othmer (1995).

A GTPase activity intrinsic to the  $\alpha$  subunit of the G protein terminates the activation. In the inhibitory pathway an inhibitory G protein  $G'_i$  is produced by analogous steps. However, the symmetry between the pathways is broken at this point, because  $G'_i$  binds with  $HR_s$ , and in this bound form  $HR_s$  cannot activate  $G_s$ . The version of the model developed in Tang & Othmer (1994) leads to a system of seven differential equations and auxiliary algebraic equations for the time evolution of the intracellular species. However, as was shown in Tang & Othmer (1995), the scheme can be reduced to four primary species for the intracellular dynamics without affecting the input-output behaviour significantly. The reduction done there leads to the network for signal transduction shown in figure 1.

There are several aspects of this scheme which have not been confirmed or are now known to be incorrect. First, the  $\alpha$  subunit of  $G'_s$  does not activate the cyclase; this is done by the  $\beta$  subunit in conjunction with a cytosolic regulator of adenylyl cyclase (CRAC) (Lilly & Devreotes 1995). As we noted in Tang & Othmer (1994), this leads to difficulties if there is an inhibitory G protein with the same  $\beta$  subunit, since the 'inhibitory' pathway would in fact not be inhibitory. Thus far the postulated inhibitory receptor  $R_i$  and the inhibitory G protein  $G_i$  have not been found experimentally, even though pertussis toxin blocks adaptation (Snaar-Jagalska & Van Haastert 1990), and it may be that there is no second pathway. This suggests that another mechanism for adaptation is employed, possibly phosphorylation of the  $\beta$  subunit (P. Schaap, personal communication), or by interference between CRAC and the  $\beta$  subunit. However, this probably does not involve a cAMP-dependent kinase, for it is known that adaptation occurs even in the absence of cAMP production (Theibert & Devreotes 1986). This kinase could be activated by the  $\alpha$  subunit or by some other mechanism that does not involve a  $G'_i$ . Some of these facts could be taken into account by changing the identity

of the species in the postulated network. For example, it is immaterial for our purposes whether  $\alpha$  or  $\beta$  activates AC if the adaptation mechanism does not involve a  $G'_i$ . Since little is known about the precise mechanism of adaptation at this point, we have chosen to retain the existing model and terminology, because it meets the primary test for a signalling model in that it reproduces the appropriate time for adaptation, the response to multiple stimuli, and the amplitudes and speeds of the cAMP waves when the cells are immobilized.

The governing equations for the intracellular dynamics are

$$\left. \begin{aligned} \frac{dw_1^i}{d\tau} &= \alpha_4 u_2^i - w_1^i - \alpha_4 u_2^i w_1^i, \\ \frac{dw_2^i}{d\tau} &= \beta_2 \beta_3 c_2 u_4^i - \beta_5 w_2^i + \beta_6 c_3 w_3^i \\ &\quad - c_3 \beta_4 u_1^i w_2^i - \beta_2 \beta_3 c_2 u_4^i (w_2^i + c_3 w_3^i), \\ \frac{dw_3^i}{d\tau} &= -(\beta_5 + \beta_6) w_3^i + \beta_4 u_1^i w_2^i, \\ \frac{dw_4^i}{d\tau} &= \gamma_1 \gamma_2 w_1^i + \Gamma_5 (1 - \Gamma_7 w_1^i) \\ &\quad - \gamma_4 \frac{w_4^i}{w_4^i + \gamma_3} - sr(w_4^i), \end{aligned} \right\} (1)$$

where

$$\begin{aligned} u_1^i &= \frac{\alpha_0 w_5(\mathbf{x}_i) + (\beta_5 - \alpha_0 w_5(\mathbf{x}_i)) w_3^i}{\alpha_1 + \alpha_0 w_5(\mathbf{x}_i) + \beta_4 w_2^i}, \\ u_2^i &= \frac{\alpha_2 \alpha_3 c_1 u_1^i (1 - w_1^i)}{1 + \alpha_4 + \alpha_2 \alpha_3 c_1 u_1^i - \alpha_4 w_1^i}, \\ u_4^i &= \frac{\beta_0 w_5(\mathbf{x}_i)}{\beta_1 + \beta_0 w_5(\mathbf{x}_i)}. \end{aligned}$$

Here superscript  $i$  designates the  $i$ th cell, whose position in the plane is denoted  $\mathbf{x}_i$ , and  $sr$  is the function denoting the dimensionless secretion rate of cAMP. The dimensionless variables above are related to the molecular species in table 1. Here  $\Gamma_5 = \gamma_5/(1+L_5) = 2.4$ ,  $L_5 = (l_{-5} + l_5^*)/l_5[\text{ATP}]$ ,  $\Gamma_7 = 1 + L_7 = 1.091$ , and  $L_7 = l_1/(l_{-1} + l_2)$ . The definitions of the variables and the parameter values are the same as those in Tang & Othmer (1995) unless otherwise stated.

The evolution of extracellular cAMP is governed by the partial differential equation

$$\begin{aligned} \frac{\partial w_5(\mathbf{x})}{\partial \tau} &= \Delta_1 \nabla^2 w_5(\mathbf{x}) - \hat{\gamma}_9 \frac{w_5(\mathbf{x})}{w_5(\mathbf{x}) + \gamma_8} \\ &\quad + \sum_{i=1}^N \frac{V_c}{V_0} \delta(\mathbf{x} - \mathbf{x}_i) \left( sr(w_4^i) - \gamma_7 \frac{w_5(\mathbf{x})}{w_5(\mathbf{x}) + \gamma_6} \right). \end{aligned} \quad (2)$$

Here  $\Delta_1 = D/k_5$ ,  $\hat{\gamma}_9 = \gamma_9 N V_c / V_0$ ,  $N$  is the number of cells,  $V_c$  is the volume of a cell,  $V_0$  is the volume of the extracellular medium,  $\mathbf{x}$  is a generic point in the plane, and  $\delta$  is the Dirac distribution. The terms on the right-hand side of the partial differential equation represent, in order, a diffusive contribution, the degradation due to external phosphodiesterase (PDE), which is assumed to be constant in space and time, the secretion of cAMP and the degradation of cAMP by membrane-bound PDE. Although we treat

cells as point sources of cAMP the secretion rate and degradation rate are first computed per unit volume (see Appendix 1), since then the equations for the local dynamics can be carried over from previous work without change. In this paper the cells only interact via the extracellular cAMP signal.

The algorithm we have developed to solve these equations can be summarized as follows. Given the initial cell states and the cell distribution, which may be uniform or random, in a square domain, and the initial distribution of extracellular cAMP we perform the following steps.

- (i) Solve the extracellular equation on a regular grid, using an alternating-direction implicit (ADI) method for the partial differential equation, lagging the secretion term.
- (ii) Interpolate cAMP from the grid to the cell positions and update the intracellular variables and the secretion by an implicit scheme.
- (iii) Update cell movement. If a cell is not moving, should it begin to move? If so, compute the direction and start movement. If it is moving, should it continue?
- (iv) Transfer the secreted cAMP to the grid and repeat the cycle.

A typical aggregation territory is approximately  $1 \text{ cm}^2$ , and the density typically ranges from  $2.5 \times 10^4 \text{ cells cm}^{-2}$ , which is the lower limit for successful propagation, to  $10^6 \text{ cells cm}^{-2}$ , the density needed to produce photographs of aggregation territories (Alcantara & Monk 1974). At the lower density limit cells are approximately  $60 \mu\text{m}$  apart if they are placed uniformly on a square grid. In step (i) above we use a grid of 201 points in each direction, and therefore a grid cell is  $50 \mu\text{m} \times 50 \mu\text{m}$ . Since we exclude cells from a strip of width one grid cell at the boundary, there are 39601 grid cells in which the cells are distributed, and at an intermediate density of 80K cells there are two cells per grid cell. If the dynamics in each cell are treated individually, as above, the computational time is large, and to reduce it we reduce the number of cells and increase their weight proportionally so as to obtain the correct production and destruction rates of cAMP. The effect of this is that we have fewer but stronger point sources of cAMP.

Reducing the number of cells and increasing their weight has little effect on the results. To support this contention we compare the one-dimensional distribution of a diffusible substance resulting from a point source of strength with one located at the centre of a grid cell with that due to point sources at  $1/4$  and  $3/4$  the length of a grid cell, each of strength  $1/2$ . The solution for the concentration in the first case is

$$f_1(x, t) = \frac{1}{\sqrt{4\pi Dt}} \exp\left(-\frac{(x-0.5)^2}{4Dt}\right),$$

Table 1. The correspondence between the dimensionless variables and the molecular species

variable	proportional to the concentration of
$u_1(t)$	stimulus receptor bound with cAMP
$u_2(t)$	activated $\alpha$ subunit of the stimulatory G protein
$u_4(t)$	inhibitory receptor bound with cAMP
$w_1(t)$	activated adenylyl cyclase
$w_2(t)$	activated $\alpha$ subunit of the inhibitory G protein
$w_3(t)$	activated $\alpha$ subunit of the inhibitory G protein bound with the stimulus receptor cAMP complex
$w_4(t)$	intracellular cAMP
$w_5(t)$	extracellular cAMP

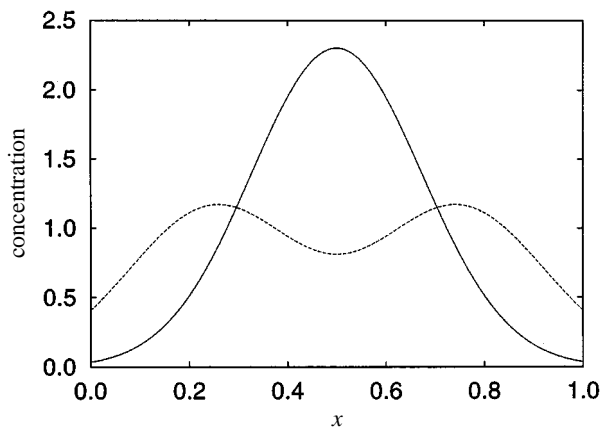


Figure 2. A comparison of the concentration profiles for a single point source (solid line) and two separated point sources of half the strength (dashed line).

whereas the solution for the second case is

$$f_2(x, t) = \frac{1}{2\sqrt{4\pi Dt}} \times \left( \exp\left(\frac{-(x - 0.25)^2}{4Dt}\right) + \exp\left(\frac{-(x - 0.75)^2}{4Dt}\right) \right).$$

These solutions are shown in figure 2, wherein  $f_1$  and  $f_2$  are evaluated at  $t = 0.0025$ . This time corresponds to half of the smallest allowable time step and gives the greatest error. The variables are scaled such that the interval corresponds to  $50 \mu\text{m}$  and the diffusion coefficient is as used in the model. The figure shows that the concentration profiles differ by small amounts at the endpoints where the diffusing grid exists. In any case, assuming a dimensionless amount 2 at the point  $1/2$  or the amount of 1 at  $1/4$  and  $3/4$ , the interpolating scheme for this one-dimensional domain gives the same cAMP, namely 1, at each of the nearest grid points. The same would be true in 2D for regularly spaced cells. Of course differences will arise when cells are not symmetrically located in a grid cell, but on the scale of several grid cells this will average out.

Another simplification used in the implementation is to combine cells when they are within a distance of  $5 \mu\text{m}$  of one another, and after doing this they are treated as one cell with twice the strength. This

is biologically reasonable since cells tend to adhere to one another when they come in contact (Siu & Kamboj 1990). Numerical tests indicate that doing this only changes the outcome of the simulations in minor ways.

A complete description of the computational procedure can be found in Appendix 2. Unless otherwise stated, the number of cells used is 10 089, each weighted by 16 according to the rules given in Appendix 1. For those computations that use a pacemaker the cells that lie within a disc of radius  $0.05 \text{ cm}$  centred at the origin have parameters which would make them oscillatory, were they to be put in a uniform suspension of the same density. This is done by decreasing the value of  $\gamma_2$  linearly from 0.4 at the centre to 0.17 at the boundary of the disc. The cells exterior to the disc are excitable but not oscillatory.

(b) Movement rules

We use two major types of movement rules. The first set is formal, i.e. not based on a model for movement, and has *ad hoc* features similar to those used by Parnas & Segel (1977) and MacKay (1978). We use it as a base against which we can compare the effects of changing these rules.

- (i) The cell moves if the time derivative of the extracellular cAMP concentration is greater than  $0.02 \mu\text{M min}^{-1}$ .
- (ii) All cells move for a fixed duration (100 s for wild-type cells) in the direction of the cAMP gradient at the cell when the motion started.
- (iii) The cell moves at a speed of  $30 \mu\text{m min}^{-1}$ .

The experimental basis for choosing these rules is as follows. (1) The threshold for the time derivative was chosen so that a triangular wave of cAMP of duration 200 s above baseline and amplitude  $0.1 \mu\text{M}$  initiates movement. (2) Cells are observed to move for about 100 s (Alcantara & Monk 1974; Tomchik & Devreotes 1981) during aggregation. However, this is undoubtedly not because there is an internal movement clock, but rather because 100 s corresponds approximately to the rising phase of the wave under typical conditions (in fact the rising phase varies between 1 and 2 min). In general, the duration will depend on the cell density and the amplitude of the wave, and in

the following section we experiment with other durations for movement. Because the cells are treated as points, the  $i$ th cell is assumed to move in the direction of the gradient of cAMP at  $\mathbf{x}_i$ . Treating the cells as points precludes evaluating the concentration around the periphery of a cell and basing the direction of motion on a rule such as ‘move in the direction of the line from the centre of mass to the point on the periphery at which cAMP first exceeds a threshold’. To deal with this limitation we are currently studying a model in which the detailed space-time profile of cAMP at the boundary, as well as the intracellular concentrations, can be evaluated (Dallon & Othmer 1997). Preliminary results show that gradients of intracellular variables such as calcium can be reliably established under typical aggregation conditions. Such gradients could then be used to guide assembly of the locomotory apparatus. As we shall see in a later section, cells can aggregate reliably even in the presence of considerable noise in the directional choice. (3) The speed of  $30 \mu\text{m min}^{-1}$  is the maximum cell speed measured in Alcantara & Monk (1974), but a more commonly observed speed is  $12\text{--}15 \mu\text{m min}^{-1}$  (Soll *et al.* 1993). If the latter speed applies throughout aggregation it would be difficult for the cells to aggregate in territories of 1 cm in about 6 h, since a cell moving continuously at  $12\text{--}15 \mu\text{m min}^{-1}$  would only move *ca.* 0.5 cm in 6 h. Yet the cells do not move in straight lines or continuously during the aggregation cycle. One explanation for the discrepancy is that the cells become more efficient in their movement with successive waves of cAMP and at different stages of their development (Varnum *et al.* 1985). Furthermore, it is known the cells move more rapidly once they form streams (Deveotes 1982). Either or both of these factors could account for the observed timescale of aggregation.

As we shall see, these formal rules can produce aggregation, but they ignore some essential biological facts. For example, as we already noted, if the profile of the cAMP wave is altered the 100 s movement rule will probably not be applicable. A detailed model of how a cell chooses the direction of motion and the length of a ‘run’ is not available, nor would it be feasible to use such a model in the present computations. However, we can develop more realistic rules based on internal variables as follows. It is known that cAMP activates the cGMP pathway via G proteins in addition to activating the cAMP production pathway (Newell *et al.* 1990). It is also known that cGMP is near the beginning of the chemotactic response pathway (Kuwayama *et al.* 1993; Valkema & Van Haastert 1994) and that cGMP production adapts to the cAMP stimulus on a timescale of about 30 s. If cGMP adapts then downstream components will also adapt, except in unusual circumstances, perhaps on a longer timescale. The identity of this downstream ‘motion controller’ is not known, but it must be used in such a way that the cell moves only when cAMP is increasing, for it is known that cells only move in the rising phase of the cAMP wave. In the absence of detailed information about the controller dynamics, we use as a stand-in a quantity in

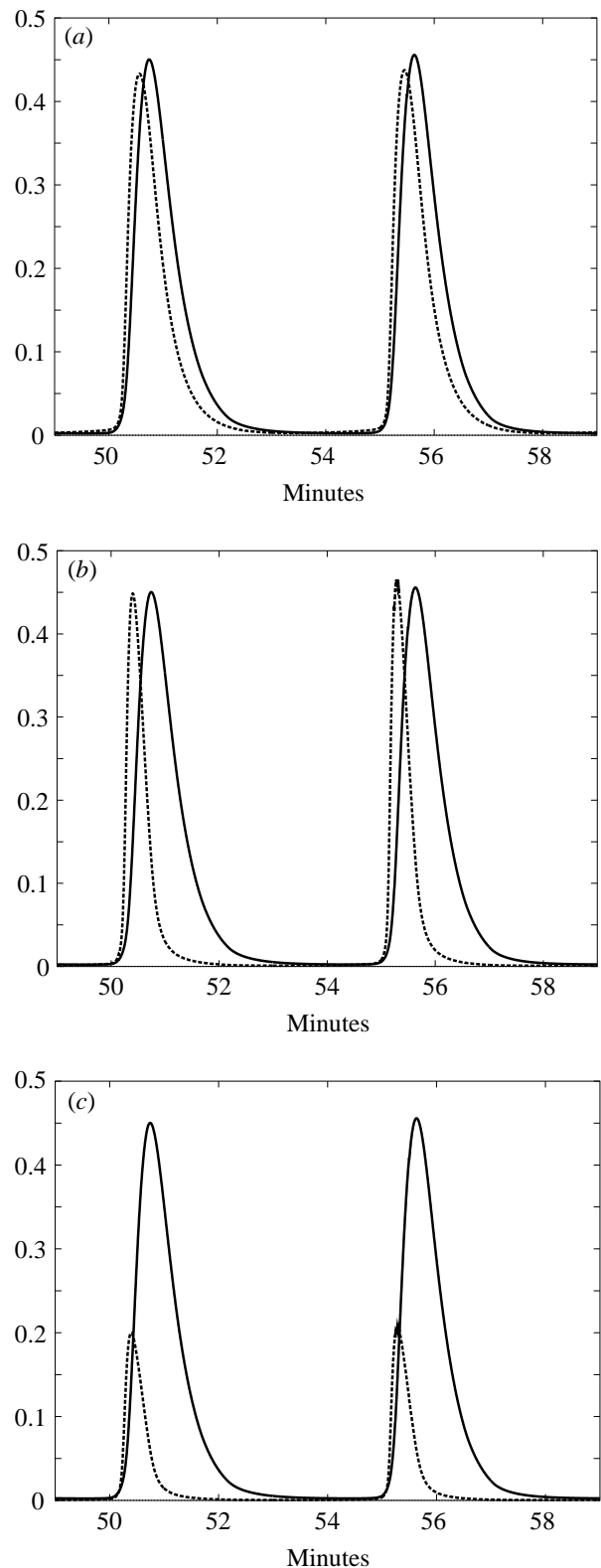


Figure 3. Several internal variables and extracellular cAMP as a function of time at a randomly chosen cell in an aggregation field. There are 80 089 cells, each weighted by 2, in the field. Throughout the solid line is extracellular cAMP ( $\mu\text{M}$ ), while in (a) the dashed line is  $w_1$ , in (b) the dashed line is  $u_1$ , and in (c) the dashed line is  $u_2$  times 5.

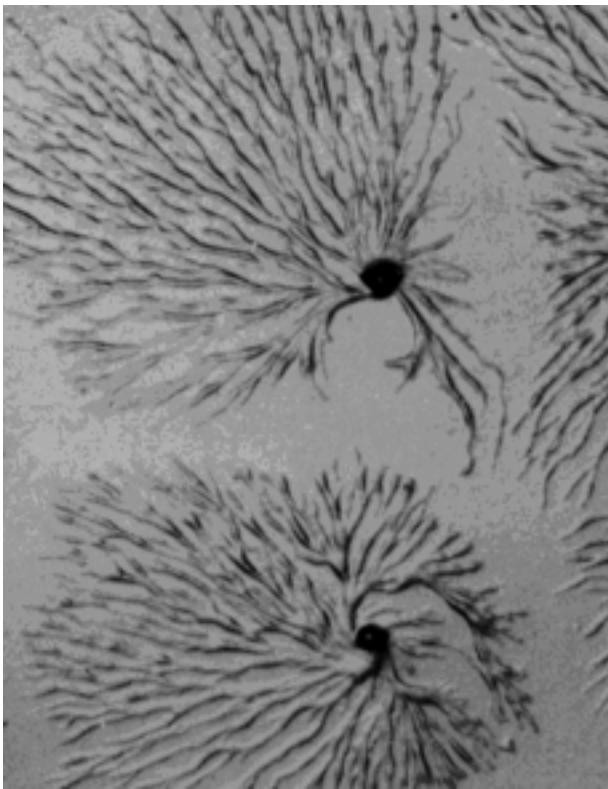


Figure 4. The aggregation pattern in a field of wild-type cells (from Loomis (1975) with permission).

the cAMP pathway that has the appropriate time-course. Suitable candidates are  $u_1$ ,  $u_2$  or  $w_1$ , and to decide which of these to use, we display their time-course at a randomly chosen cell in figure 3, along with the cAMP concentration at that cell. One sees in figure 3*a* that  $w_1$  is probably not suitable if the rule is that motion persists only as long as  $w_1$  is increasing, since motion would cease before the peak of cAMP reaches the cell. However, the gap between the cAMP and  $w_1$  peaks is small, and it is not known that a cell stops precisely as the peak of the wave passes. One sees in figure 3*b, c* that either  $u_1$  or  $u_2$  could be used if the rule is that motion persists as long as these variables are above a suitable threshold, and we have chosen to use the time-course of  $u_2$  to determine cell motion.

These considerations lead us to the second set of movement rules, which we designate the ' $u_2$ ' rules.

- (i) The cell moves if the dimensionless concentration of  $u_2$  is greater than 0.004.
- (ii) The cell moves in the direction of the gradient of cAMP when the motion was started.
- (iii) The cell moves at a speed of  $30 \mu\text{m min}^{-1}$ .

We do not incorporate a diffusive component of motion in either set of rules because it is observed that this component is small and is suppressed when the cell receives a superthreshold chemotactic signal. In the following sections we present simulation results

from the model which show that aggregation patterns for both wild-type and for mutant cells can be reproduced, and we present results on the effects of changes in density, the excitability, the fraction of pacemakers present, and the directional sensitivity on the aggregation patterns.

### 3. RESULTS FROM SIMULATIONS OF THE MODEL

#### (a) Experiments with different movement rules

The first set of computational experiments is aimed at understanding the effect of changes in the duration of movement. These experiments use three fixed durations: 20 s, the nominal 100 s, and 500 s. The first value was chosen because it has been shown by Futrelle *et al.* (1982) that cells can alter their direction within 20 s after the location of a source of cAMP is changed. Thus there is no long-term (greater than 20 s) persistence in the motion, and the question arises whether the artificial mutant, *jittery*, which can change direction every 20 s, aggregates. The rationale for the second duration has already been discussed, and the third duration is intended to mimic the behaviour of the *streamer F* mutants, which move five times more slowly than normal cells (Ross & Newell 1981). The results of the simulations are shown in figure 6.

These results are to be compared with the wild-type aggregation pattern shown in figure 4. A comparison of this figure with figure 6*b* shows that a duration of 100 s produces large-scale aggregation patterns that are similar to those observed for wild-type cells. This is not unexpected, because we know from earlier work that the model for signal transduction and relay produces the correct secretion rate, and that the cAMP waves have the correct amplitude and duration when the cells are immobilized (Tang & Othmer 1994, 1995). Thus this comparison can be regarded as one more check on the model, albeit a much weaker one than those used in previous work. As we shall see later, other movement rules produce even better correspondence between the model results and the experimental observations.

The cells which move for 500 s form fewer but larger and more compact streams (figure 6*c*). These results are in agreement with experimental data, which shows that the *streamer F* mutant forms long streams and larger aggregation territories (Ross & Newell 1981). One can see in figure 6*a* that the aggregation pattern is quite different for *jittery*. There are certainly hints of stream formation, and the branching pattern shows some similarity with that in figure 6*b*, especially in the upper left-hand quadrant. However, there is little long-range aggregation, the streams are fragmented, and aggregates are small and highly localized.

The differences in the aggregation patterns shown in figure 6 are not due to differences in cell density or initial conditions, nor do they stem from differences in the cAMP waves in the early stages: the underlying waves for each simulation started out identical

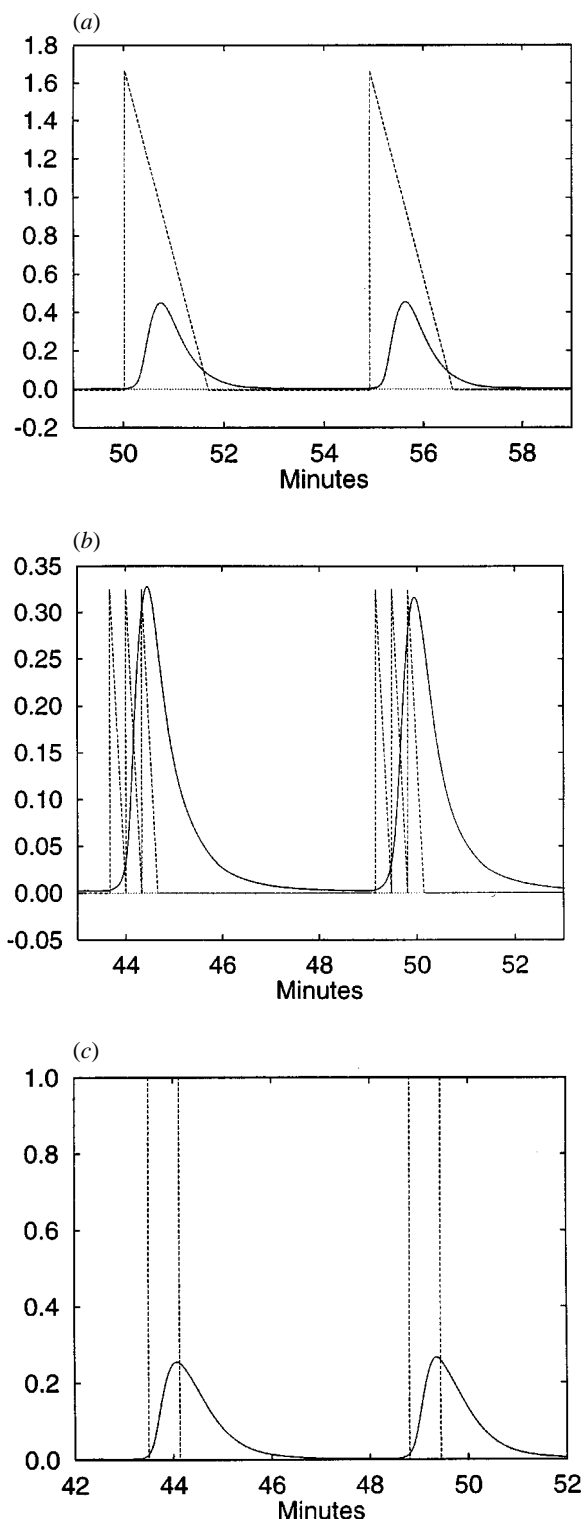


Figure 5. Extracellular cAMP ( $\mu\text{M}$ ; solid line) and the amount of time remaining on the movement clock in minutes (dashed line) are shown in (a) and (b) for a randomly chosen cell in an aggregation field. In (a) the cells move for 100 s and in (b) they move for 20 s. In (c) the motion is determined using the  $u_2$  rules. The solid line shows extracellular cAMP and the dashed line is 1 when the cell is moving and 0 otherwise. In all cases there is a pacemaker at the centre, and the density is 0.2.

and changed only as the aggregation patterns were established. In all cases the waves have virtually the same duration of elevated levels of cAMP. Thus we conclude that the differences stem from the different movement durations.

In order to better understand the results of the 20 s movement rule, we display the external cAMP concentration and the amount of time remaining for movement in a cycle in figure 5. Obviously cells which only move for 20 s must go through three cycles of movement and possibly re-orientation during the 60 s interval in which the major increase of cAMP occurs at the leading edge of the wave. Because there are multiple localized sources of cAMP, the amplitude of the cAMP waves varies rapidly in space, as is shown at a fixed instant in figure 10. From this one sees that if the cells adjust their course during the passage of a wave they have a high probability of moving in the wrong direction, and in particular, of moving toward a receding wave. This is the familiar 'back-of-the-wave' problem, which here accounts for the relatively fragmented character of aggregation in figure 6a. When that simulation is run for a longer period one finds that the streams break into many small aggregates. The relative ineffectiveness of aggregation when cells may re-orient every 20 s suggests that either the cells do not undergo several distinct 'runs', i.e. several quantized cycles of movement and re-orientation, during a global cAMP wave, as was conjectured by Soll *et al.* (1993), or that other mechanisms such as cell polarization or adaptation in the transduction step are at work.

The need for other mechanisms can be understood by noting that there are two space scales involved in the cAMP distribution, one characterized by the small-scale local variations that arise from the localized bursts of cAMP emitted by cells, and a longer one characterized by the wavelength of a locally smoothed version of the cAMP wave. The cell sees only the small space scale, yet the foregoing simulations show that aggregation is more effective if the cell in effect takes a 'longer view'. Rather than simply imposing this longer view in the form of a rule using longer runs, we can either build some polarity into the movement process, or incorporate adaptation into the transduction process. Polarization of the movement is essentially equivalent to imposing longer runs, but has a firmer biological basis. In the form we later incorporate it, adaptation turns off the movement when cAMP is decreasing and automatically solves the back-of-the-wave problem for a cell.

Evidence that Dd cells polarize in the presence of chemical gradients of cAMP was reported by Varnum-Finney *et al.* (1987), and we incorporate polarity into the movement rules as follows. If the cell has not been moving in the previous time step and the time derivative of cAMP is superthreshold, it moves in the direction of the local gradient. If the cell has been moving, the next move is in the direction given by the vector sum of two thirds of the old direction and one third of the direction given by the local gradient. In either case the run length is maintained at 20 s. With cell polarization built into

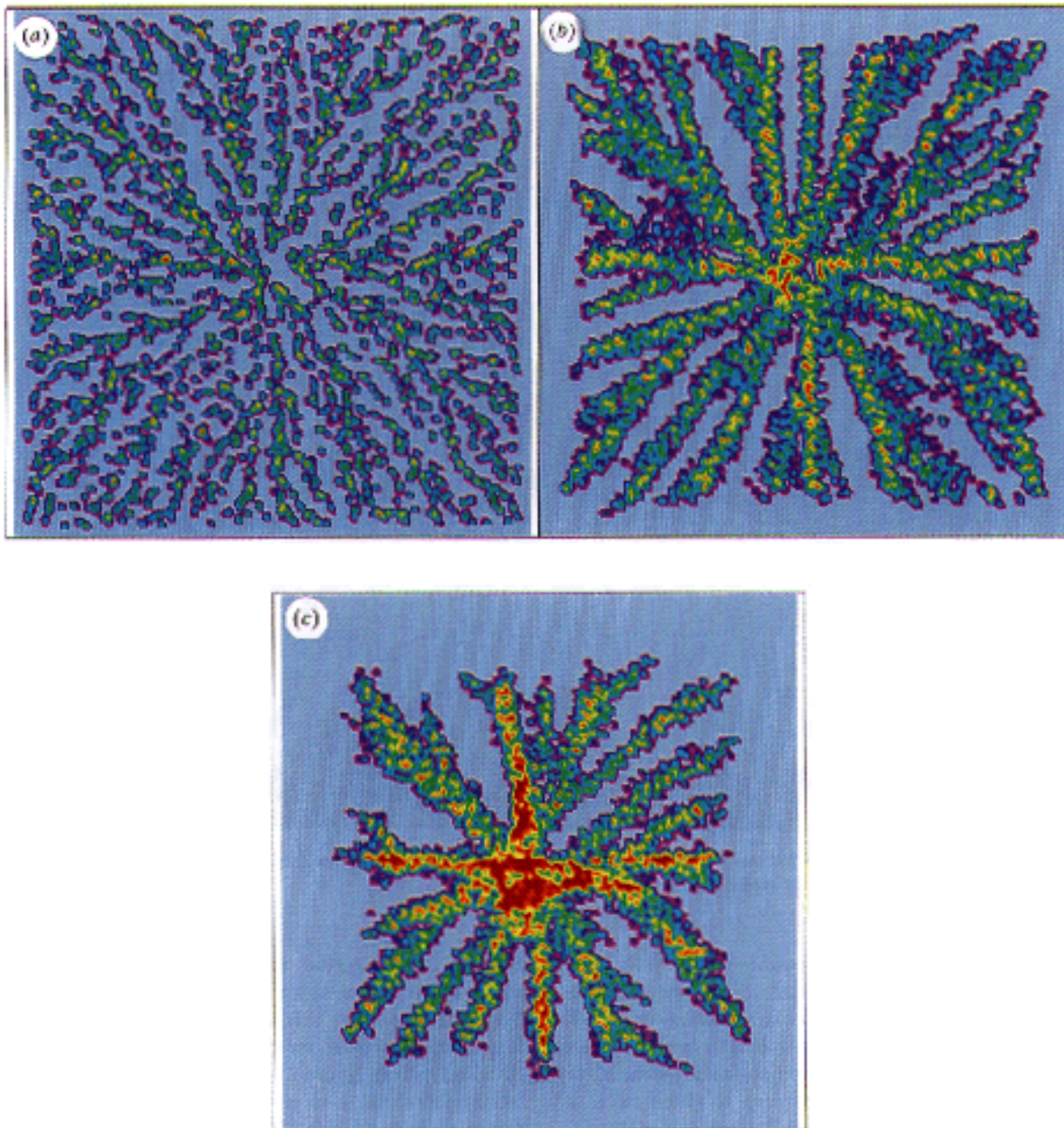


Figure 6. Aggregation patterns for simulated mutants and wild type cells. The aggregation patterns shown are: in (a) for the *jittery* mutants with movement duration 20 s, in (b) for the wild-type cells with a movement duration of 100 s and in (c) for the *streamer* F mutants with a movement duration of 500 s. The final time is 95 min, and cell densities greater than or equal to 1 are shown in red. (A cell density of 1 represents approximately  $800\,000\text{ cells cm}^{-2}$ .) Cells in the centre are oscillatory with  $\gamma_2$  ranging between 0.4 and 0.17.

the movement rules, the resulting aggregation pattern contains more streams, each of which is smaller and more highly branched when compared with the pattern that results from using a run length of 100 s (cf. figure 6b and figure 7). This aggregation pattern appears to better match the experimentally observed patterns shown in figure 4.

From figure 7 one can conclude that polarization of the cells can overcome the fragmentation of aggregation that results when cells re-orient several times during a wave. However, there are cell types which lack myosin II and as a result do not polarize well, but which still form streams and aggregate (Wessels *et al.*

1988). These cells exhibit chemotactic behaviour, but they are less efficient in their movement than normal cells. In another mutant, which attaches to the substratum very strongly and also does not polarize well, streams form and aggregation is successful, and the patterns of aggregation are only slightly different from wild-type cells (Claviez *et al.* 1986) (figure 8). These two mutants demonstrate that polarization is not necessary for successful aggregation.

From the foregoing simulations we learn that if cells use a fixed run length, then in the absence of polarization they must use a sufficiently long run to aggregate successfully. If cells polarize in the manner

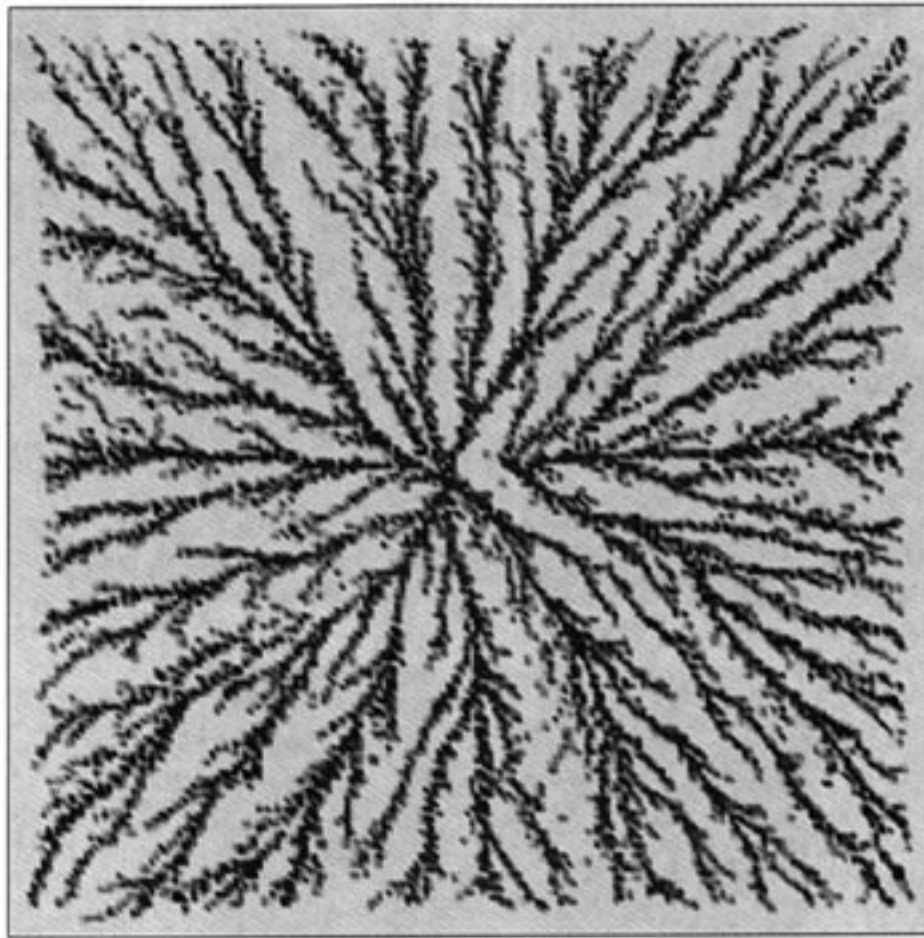


Figure 7. Aggregation patterns for polarized cells using a 20 s run length. The aggregation pattern is shown at 95 min and cell densities greater than or equal to 1 are shown in black.

described above they can aggregate successfully even if the run length is quite short. Since the mutants demonstrate that polarization is not necessary, they must either use a long, fixed run length or some other mechanism. An alternate mechanism is encoded in the  $u_2$  movement rules. According to these rules, if the intracellular motion controller exceeds a threshold the cell moves in the direction of the local gradient, and continues to move as long as the controller remains above threshold. By hypothesis, this controller adapts to constant extracellular cAMP levels and thus will only exceed a threshold when the extracellular cAMP levels are rising sufficiently rapidly. The results of a simulation that uses these rules are shown in figure 9. The aggregation pattern compares very well with both the result using polarized movement (figure 7) and the wild-type aggregation pattern shown in figure 4.

One can see from figure 5 that the total duration of movement in a passing wave is approximately the same, whether the cell uses the  $u_2$  rules, the polarized rules, or the *jittery* rules. What is different is how cells choose their direction of movement. In this respect figure 5 is incomplete, for it does not show the local gradient at the cell. If the wave is essentially planar at the cell then all three rules will lead to a similar pattern of motion. However, this is rarely the case,

for as we noted earlier, the cell sees the composite of many small waves which emanate from nearby cells. To clarify the effect this has on cell motion when different rules are used, we show the cell paths of five individual cells in figure 11. An overlay of these figures would show that each of the cells starts at the same point in the five figures. Note that cells which use the  $u_2$  rules have the smoothest paths, since they only make a directional choice about 30 times, while cells which use the *jittery* rules have the roughest paths since they make 90 decisions. The three lower right cells in the *jittery* mutant seem to be converging to a point rather than entering a stream as in the other simulations. Cells using a 100 s run length almost get trapped at roughly the same point in space, but are able to escape this region. Those using a 500 s run length frequently double back across streams, but this would not occur if we incorporate the fact that cells in a stream adhere to each other. These tracks help to clarify the macroscopic patterns shown earlier. Generally speaking, the longer run lengths lead to more compact streaming, but individuals back-track much more than with a shorter run length. As we observed earlier, the *jittery* mutant results in a fragmented pattern of many local aggregates, which is not observed in experiments. The  $u_2$  and polarized rules produce a much more ramified aggregate, with

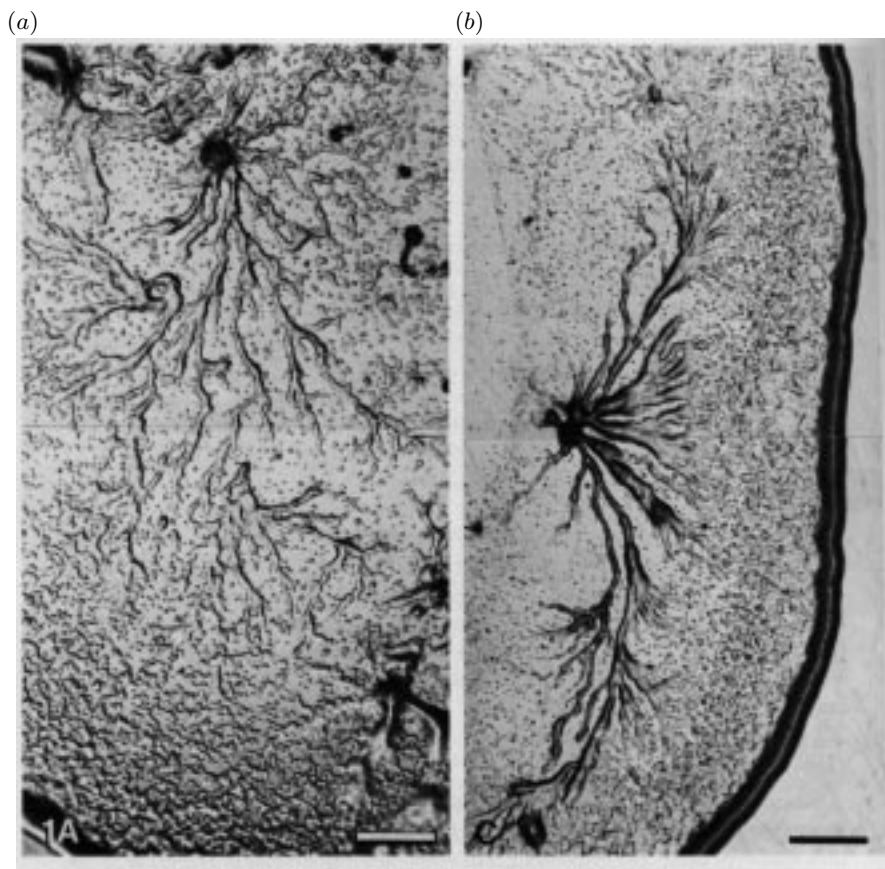


Figure 8. Normal cell aggregation patterns (a) and an aggregation pattern of mutants with flattened cells (b). The scale bar shown is 0.5 mm. (From Claviez *et al.* (1986), with permission.)

many small branches. These aggregates are the most comparable with the experimentally observed ones.

As we remarked earlier, it is known that cGMP adapts and that it is involved in the locomotory machinery, probably via control of the calcium levels in the cell. Thus the  $u_2$  rules seem more realistic biologically, but since it is also known that cells polarize this probably also plays a role in wild-type cell aggregation. Either set of rules can effectively overcome the back-of-the-wave problem discussed in Soll *et al.* (1993), but the  $u_2$  rules are more reliable in this regard. If the  $u_2$  rules are used, changes in the amplitude and duration of the cAMP wave will change the chemotactic response, in that the cells will move for a longer or shorter period of time. Observing the cells' behaviour in response to a variety of wave amplitudes and durations would help to clarify the movement rules used.

#### (b) *The effects of AC activity on patterns of aggregation*

The next aspect to be investigated is the effect of changes in the excitability of the cells or in their basal cAMP production rate. The excitability can be changed experimentally by adding caffeine to an aggregation field, as was done by Siegert & Weijer (1989). This has several effects, one of which is to enhance formation of cores that are free of cells, around which a stream of cells migrates (these are also seen occasionally in untreated fields). The size

of the core is directly proportional to the amount of caffeine added. It is speculated by Siegert & Weijer (1989) that core formation is enhanced because caffeine lengthens the period of the cAMP wave. In an earlier model the caffeine effect was on intracellular calcium, which inhibited the cyclase (Monk & Othmer 1989*a*), but here its effect is simulated by lowering the value of  $\gamma_2$ , which is normally set at 0.17. (Recall that  $\gamma_2$  is a measure of the activity of the activated adenylyl cyclase.) In the following simulations a spiral wave is started as described in the figure caption. When  $\gamma_2$  is too low ( $\gamma_2 \lesssim 0.12$ ) the cAMP waves do not propagate at all, and for  $\gamma_2 = 0.13$  the tip of the spiral wave meanders, never anchoring to a spot or rotating around a fixed core. The results for three values of  $\gamma_2$  which produce stable cores are shown in figure 13.

One sees there that cores form in all cases, even using the 'standard' value of  $\gamma_2$ , and that their diameter increases as  $\gamma_2$  is decreased. Core formation has been investigated in another context by Monk & Othmer (unpublished work; 1989*a, b*), who showed that the core size in a FitzHugh–Nagumo system is primarily determined by the excitability of the system, but it is difficult to obtain a quantitative relationship analytically. The cores shown in figure 13 are of the same magnitude as those observed experimentally (cf. figure 15). One also sees in the figure that changes in excitability change the number of primary streams around the core. An increase in the excitability pro-

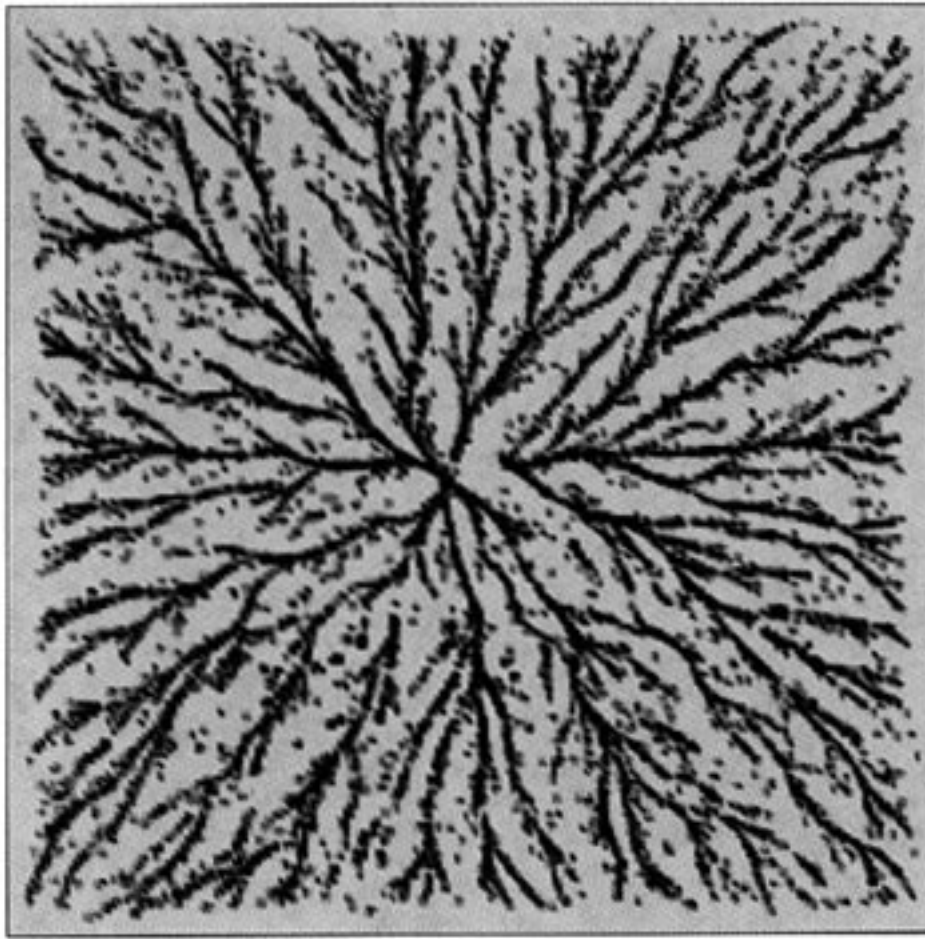


Figure 9. An aggregation field in which the cells move according to the  $u_2$  rules. The aggregation pattern is shown at 95 min and cell densities greater than or equal to 1 are shown in black.

duces a tighter spiral cAMP wave, more compact cell streams, and fewer primary streams near the centre. The far-field structure of the aggregation pattern is similar for all three simulations, even though the far-field wavelength of the cAMP wave will vary with the excitability. When the spiral is far from the core in an aggregate with well-defined streams, the wave is essentially many independent pulses travelling down the individual streams (cf. figure 14).

Our computations show that the cores collapse after *ca.* 300 min of the simulations (see figure 12), as is also observed experimentally (Durston 1974). This is probably due to the fact that the normal direction to the level curves of the cAMP wave does not coincide with the normal direction to the circumference of the core. As a result, there is an oblique component to the direction of cell movement which will ultimately lead to the collapse of the core.

The results shown in figures 12 and 13 can be compared to experimentally observed patterns of *Dd* aggregations with and without caffeine in figure 15.

In another experiment, cells are altered so that they over-express ACG, a constitutively active adenylyl cyclase that is unregulated by cAMP (Pitt *et al.* 1993). As a result, these cells have a greater basal production rate of cAMP. It is observed experimentally that in *wt/ACG* aggregation fields, the

cells initially begin to stream as they normally do, but then the streams break up into small mounds which form fruiting bodies (Pitt *et al.* 1993). We can simulate the *wt/ACG* dynamics by adding a constant to the equation for the time derivative of  $w_4$  (the intracellular cAMP) for each cell, for in that way the basal level of cAMP production is increased. The result of a simulation using these equations is shown in figure 16. One observes several local mini-aggregates that display normal morphology. We believe that the local ‘organizers’ of these aggregates arise as follows. Because all cells produce more cAMP, regions of higher cell density can act as pacemakers and organize local regions, whereas in previous simulations the parameters were such that this did not occur. This conjecture is borne out by a later simulation in which many pacemakers are dispersed throughout the field (cf. figure 19). This phenomenon also occurs in other species such as *Polysphondylium pallidum* and *Dictyoselium polycephalum* (Raper 1984).

### (c) *The effects of density on aggregation patterns*

We have shown in §3*a* that changing the movement rules can have a dramatic effect on the aggregation patterns. In this section we examine the effect of cell density on these patterns. First, we consider a set of simulations in which the initial cell and cAMP

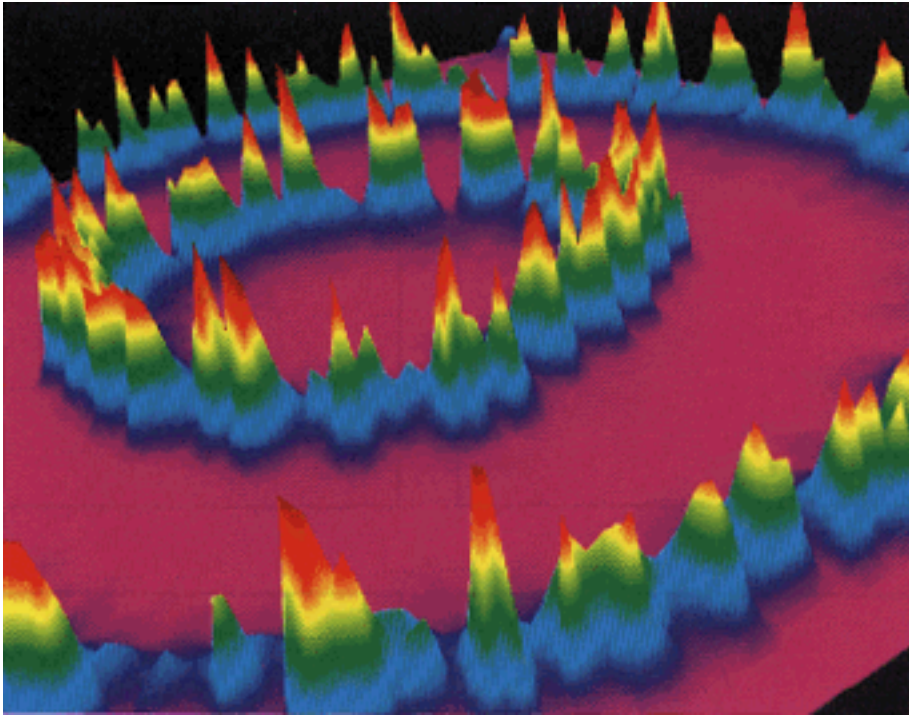


Figure 10. The cAMP concentration in the aggregation field at a fixed instant in time. The volumetric density is 0.4 and the colour is scaled from red to magenta where red corresponds to cAMP concentrations greater than  $1 \mu\text{M}$  and magenta corresponds to concentrations equal to 0.

distributions in the aggregation field are uniform and in which there is a pacemaker region in the centre. If the initial density is relatively low (*ca.* 0.15 or about 120 000 cells) the cAMP waves do not propagate after about 90 min. The reason for this failure is that a gap in the cell density appears at the boundary of the pacemaking region (results not shown). The break in density results from the fact that cells in the pacemaker region experience a cAMP wave that is broader and of larger amplitude than in the excitable region, and therefore they move longer by virtue of the  $u_2$  movement rules. The cells which comprise the pacemaker continue to move and reorganize after the waves stop propagating beyond the pacemaker region. The occurrence of such a break is the result of having a uniform initial density and a sufficiently large pacemaker region; when random initial conditions are used no breaks are observed. These breaks are also not observed experimentally, but it may be possible to observe them if care is taken to distribute the cells uniformly, and to create a large enough pacemaker region in the centre.

However, the fact that the breaks only occur for uniform initial distributions gives insight into the mechanism of stream formation under normal conditions. Our conjecture, which is supported by simulations to be described shortly, is that stream formation is the result of sufficiently large variations in the initial distributions of cAMP or cell density, or in non-uniform parameters in the cell population. We believe that an initially uniform aggregation field, comprised of identical cells, in which travelling cAMP waves propagate outwards from a pacemaker

region, is stable to small perturbations, in contrast to what has been found in model systems by others. Said otherwise, we believe that stream formation requires finite-amplitude disturbances.

It is easy to produce a heuristic argument that shows why the uniform cell distribution should be unstable to sufficiently large disturbances. Cells move in the direction of higher cAMP and produce it as well; therefore a disturbance that creates a large enough density or cAMP non-uniformity will induce cell movement, which will reinforce the non-uniformity, and so on. It is perhaps more difficult to see why a uniform field should be stable to small disturbances, but there are several reasons. First, it is known that there is a diffusional component to cell motion, and this will tend to stabilize the uniform distribution. Diffusion is not explicitly included in our model, but it can be shown that the numerical procedure introduces it via the truncation errors in the interpolation of cAMP back and forth from grid to cells. Secondly, it is known that the transduction pathway to the locomotory machinery adapts to the extracellular cAMP signal, and this fact is included in our model. As a result of adaptation, disturbances that vary slowly over time will not be amplified by cell movement. Finally, there is a threshold in the cAMP gradient of *ca.*  $10 \text{ nM mm}^{-1}$  (Fisher 1990) below which the cells do not chemotact. These three factors, diffusion, adaptation and a threshold, all mitigate against amplification of small disturbances.

Other numerical evidence that supports our conjecture is as follows. In a simulation with a uniform initial cell density of 0.2, streaming occurs after a

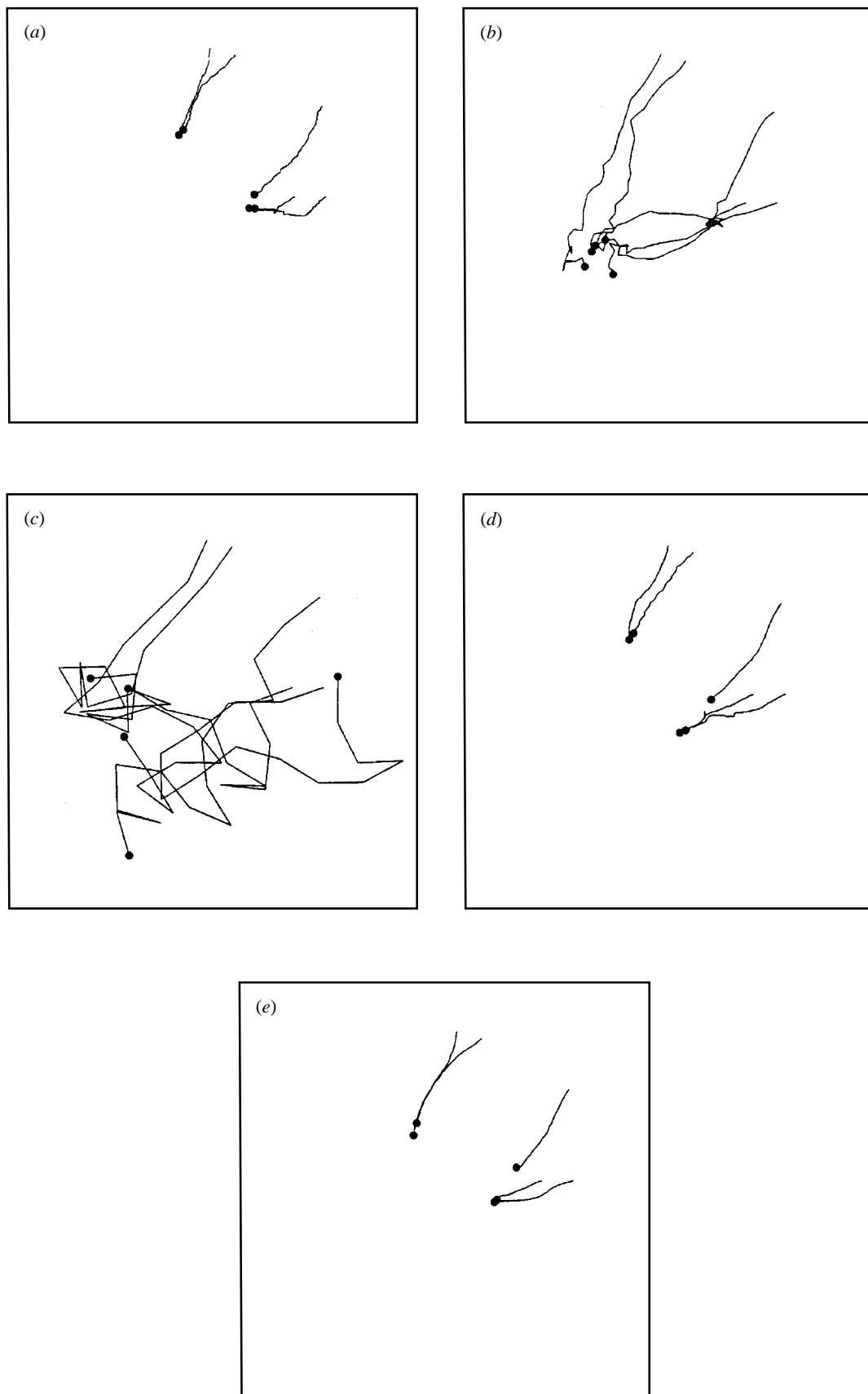


Figure 11. A microscopic view of aggregation showing five cell tracks. Paths in (a) are for the *jittery* mutant, in (b) cells use a 100 s run length, in (c) the 500 s *streamer F* rules, in (d) cells are polarized and move for 20 s, and in (e) cells move according to the  $u_2$  rules. The paths are shown for  $t \in [0, 150]$  min. The circles denoting the cells have a radius of  $20 \mu\text{m}$ ; thus cells do not coalesce according to the rule described earlier until the overlap is sufficiently large. The domain shown is approximately  $0.235 \text{ cm}$  on a side.

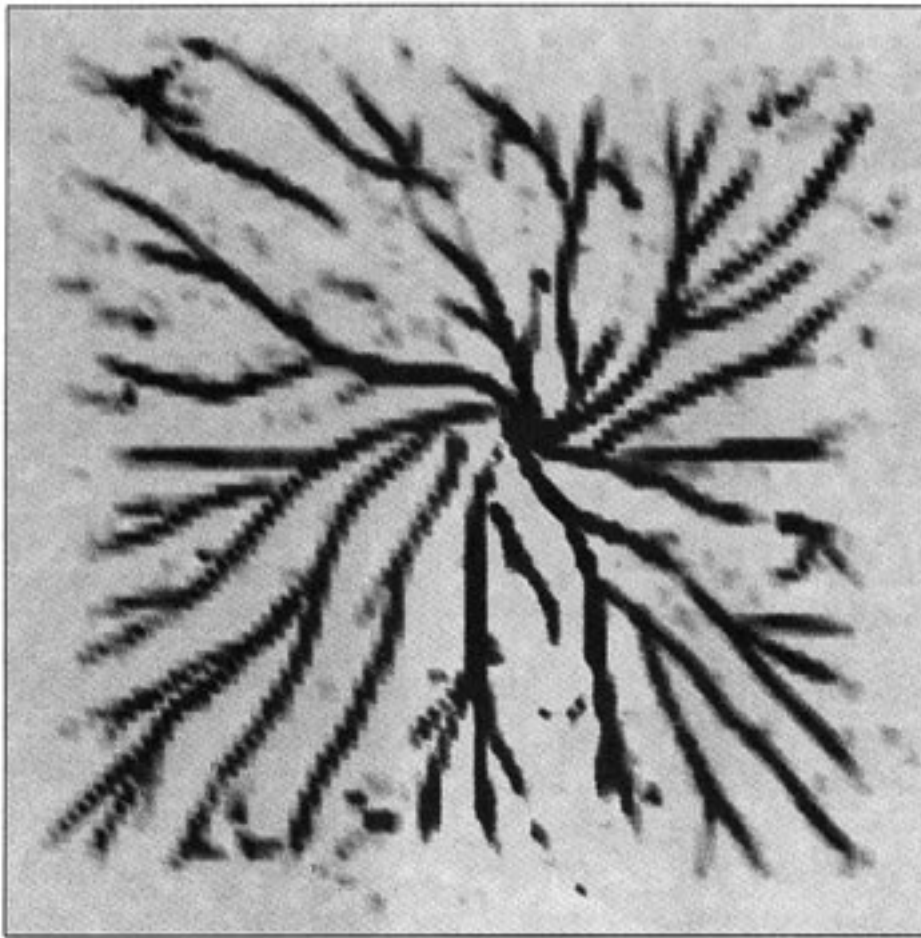


Figure 12. The cell density in the aggregation field shown in figure 14 at a later time ( $t = 400$  min). Note that the core is completely filled.

period two to three times longer than in the case with random initial density. Because the streams form along the grid lines first and display none of the branching structure seen using non-uniform initial conditions, we believe that the streaming is due to grid effects and the accumulation of round-off error. In order to test this hypothesis we did a simulation on a cylinder with a band of pacemaker cells wrapped around it at  $x = 0.5$ , where  $x \in [0, 1]$  is the axial coordinate. The initial conditions were uniform around the cylinder and the cells that are within 0.05 cm of the centre were made oscillatory by giving them values of  $\gamma_2$  which range from 0.4 to 0.17. (In all the simulations referred to in this section the number of cells used was 40 602 each being weighted by either 3 or 4 depending on the initial density.) In this simulation the cells moved toward the centre line, uniformly in the transverse direction, for at least 100 min, i.e. there was no streaming before this time. After this time the pacemaker region begins to break up, which causes streaming in the nearby field. The far-field structure remains largely unaffected for at least 50 min more. In figure 20 we show the results for this simulation, and for comparison, a simulation using a random initial cell distribution. One can see there (note the different density scales for the figures) that the streaming patterns are well established in

the latter case long before the break up begins to occur in the uniform case. Thus we conclude that linear instabilities, if they exist at all, do not effect the aggregation patterns on a timescale that is relevant to aggregation under normal conditions.

This conclusion contradicts the conclusion reached in Levine & Reynolds (1991) for a different model, which is that streaming is due to a linear instability in the governing equations. These authors use a continuum description and show that planar travelling waves can be unstable to perturbations of wavelengths greater than approximately 8 mm, but stable otherwise. They conclude that streaming instability can occur, but their results show that it is a very long wavelength instability and thus would probably not be seen on the scale of normal aggregation patterns. In our model, small amplitude perturbations do not grow, either when travelling waves are initiated with a forcing function on a domain with uniform initial density (results not shown), or when a pacemaker initiates aggregation. Instead, the streaming in our model seems to be initiated by variations in density or other factors. When a random initial cell distribution is used, the density variations tend to be reinforced globally, whereas when uniform initial conditions are used the far-field density variations are driven by variations which originate in the pacemak-

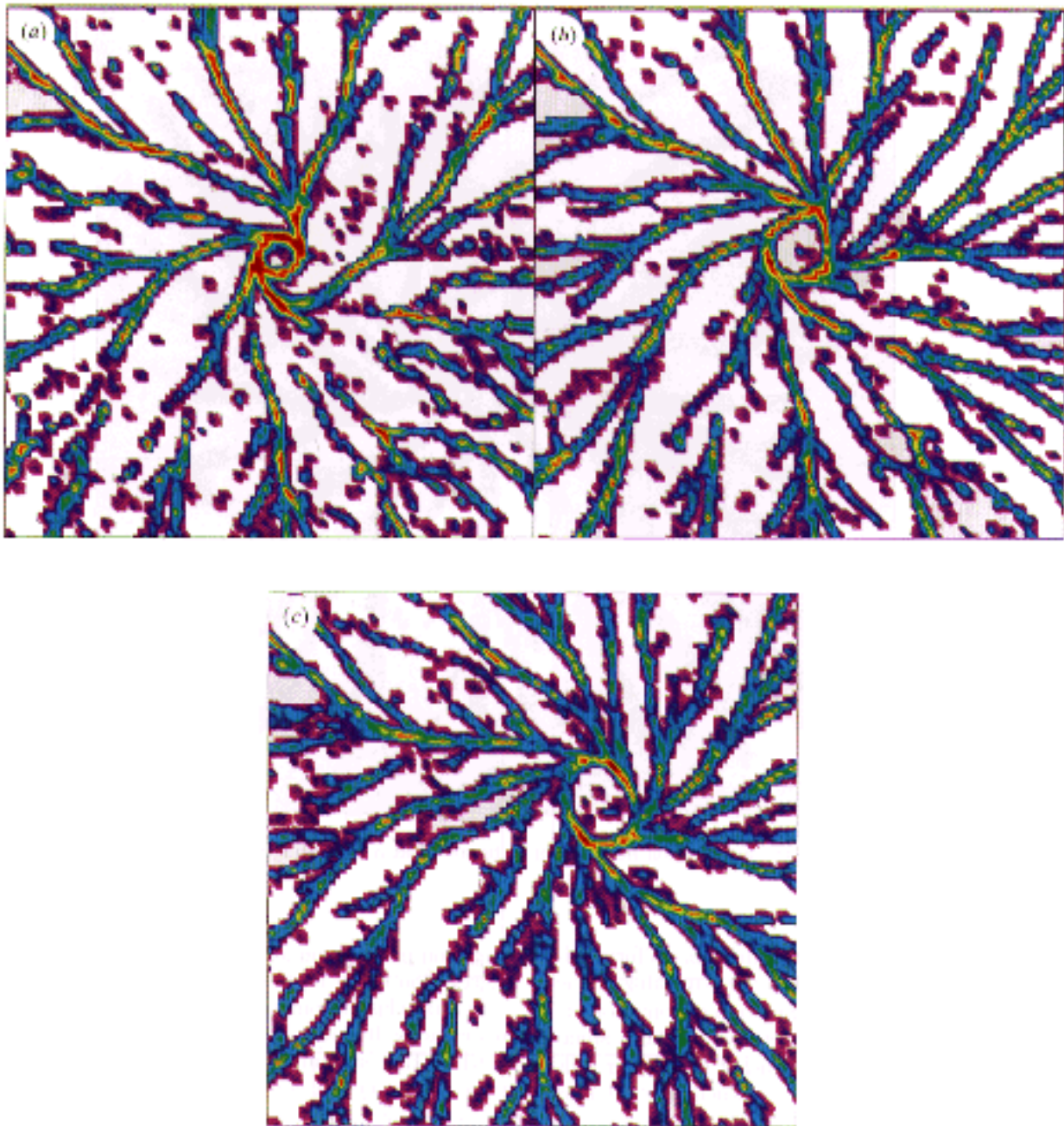


Figure 13. Aggregation patterns under changes in the excitability. In (a)  $\gamma_2 = 0.17$ , in (b)  $\gamma_2 = 0.155$ , and in (c)  $\gamma_2 = 0.14$ . The pattern is shown at 150 min, cell densities greater than 1.5 are shown in red, and cells move according to the  $u_2$  rules. A spiral wave was initiated in a 1 cm square domain by elevating cAMP in a strip extending from the centre to one side, and imposing a refractory region behind it. The central square of side 0.5 cm is shown. The full field corresponding to (c) is shown in figure 14.

ing region. This is understandable since the variations in density will be reinforced with each passing wave of cAMP: thus the denser areas will produce responses of greater amplitude, thereby causing cells to move towards those areas and increasing the density there further.

Two additional simulations were done on the cylinder in order to determine the sensitivity of stream formation to the amplitude of perturbations of the initial cell density and the cAMP concentration. In these simulations we began with uniform conditions in the  $y$  direction except in a small strip near the centre. We found that an initial density variation of

5% or more in this strip grows in time and streams are formed. Streaming is also initiated if the central strip is paced periodically and there is a variation of at least 5% in the amplitude of the cAMP forcing function. Thus variations in either the cAMP concentration or the density can cause streaming. This contrasts with the conclusion of Vasiev *et al.* (1994), who assert that stream formation is primarily the result of the dependence of cAMP wave speed on the cell density. It also shows that a random initial cell distribution is sufficient for streaming, but it is not necessary, as was claimed by Vasiev *et al.* (1994). Stream formation is influenced by many factors, in-

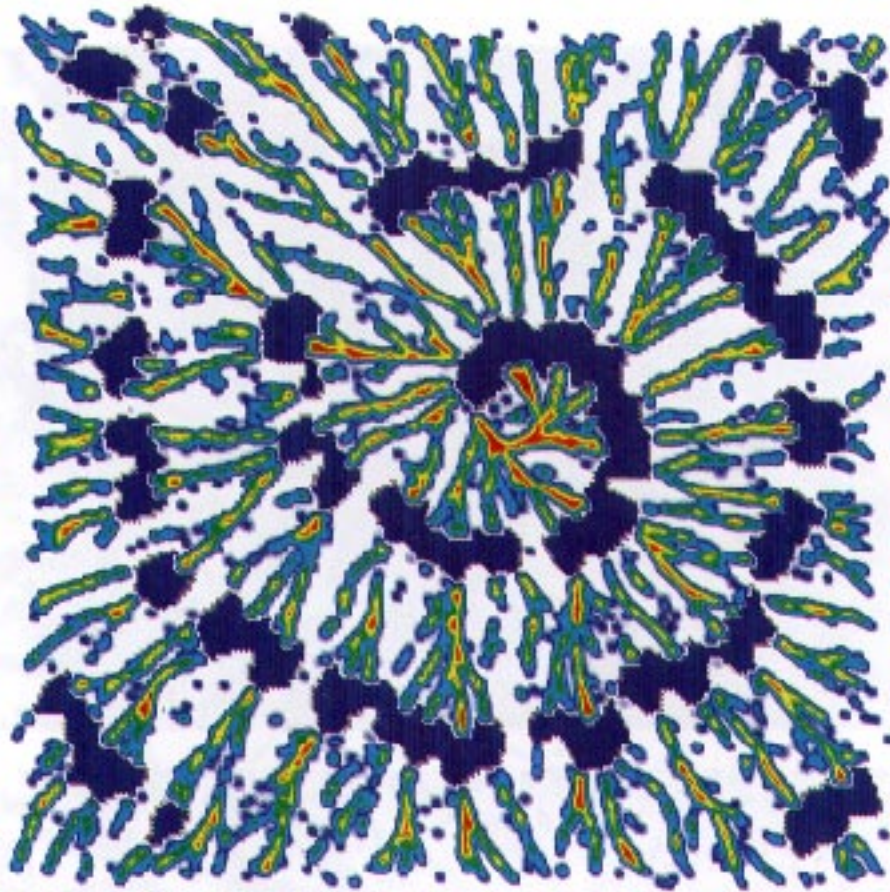


Figure 14. An overlay of the cAMP wave and the density plot for  $\gamma_2 = 0.14$  (cf. figure 13c). The cAMP wave is plotted if the concentration is greater than 0.1 micromolar (dark blue), and cell densities of one or greater are shown in red.

cluding density variations and cAMP concentration variations. Each of these has effects which tend to reinforce streaming. The questions which remain are which mechanism, if any, is the dominant one, and whether there are any other important factors, such as variation in cell speeds, and variations in other cell parameters, such as the amount of adenylyl cyclase.

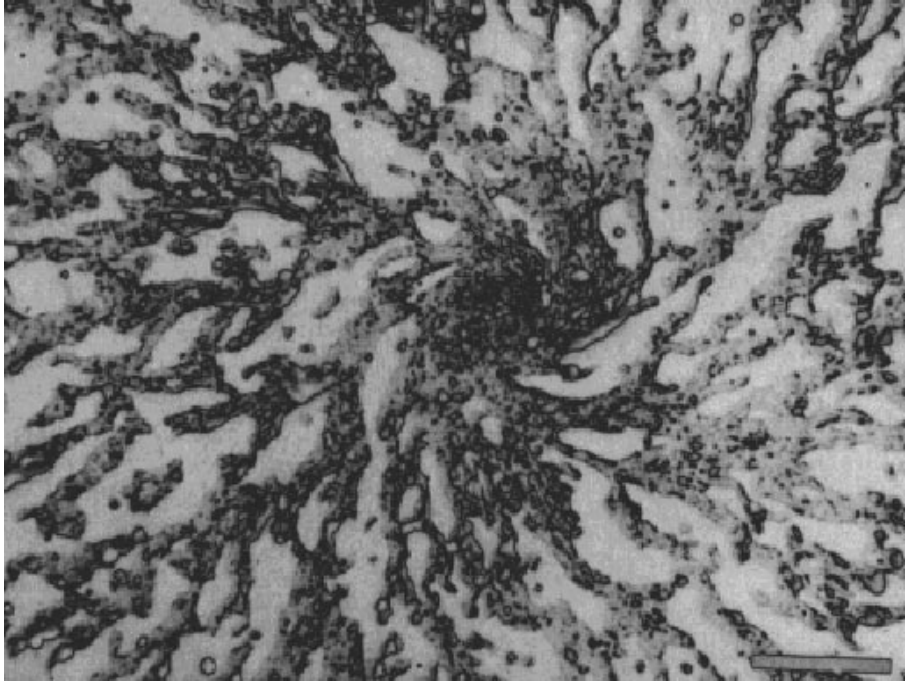
#### (d) *Formation of spiral waves*

Spiral waves are the dominant pattern of aggregation in many laboratory experiments, but it is not understood how they arise. As we showed earlier, they can be initiated using special initial conditions, but we have also found that they can arise spontaneously. Using a random initial cell density, we find that they are generated by a pacemaker that initiates axisymmetric (target pattern) waves which can break up into a spiral when they encounter a low density region. We discovered that spirals do not form when the initial density is too low, but they do form at a sufficiently high density ( $\rho \geq 0.4$ ) (cf. figure 17). These spirals initially coexist with the nearest pacemaker, but eventually they entrain it. Recent laboratory experiments also suggest that the average density is an important factor in the formation of spirals (Lee *et al.* 1996). Our computational experiments, which were done before learning of these results, support these findings. To understand the density effect

we must understand two aspects: (i) how spiral waves are initiated, and (ii) when can they coexist with a pacemaker.

Durston (1974) was one of the first to consider theoretically how waves can be broken during aggregation, and Lee *et al.* (1996) observe that spirals form at disrupted wave fronts that arise from wave-wave interactions and from inhomogeneities in the system. However, it is not understood why density is an important factor in determining whether or not spirals will form. In our simulations wave-wave interactions are not important, since there is only one pacemaking region. At low average densities a local low density region usually elongates in the direction of propagation as streams form on either side of the region. Initially the cAMP wave will start to curl as it travels around the region on both sides, but then the two pieces rejoin at the rear to form a distorted, yet connected wave front. At higher average densities our computational results suggest that passive spread of cAMP through the low density region is rapid enough to trigger a wave on the downstream side of the low density region before the main wave reaches that side. Initiation of this secondary wave can then alter the cAMP environment sufficiently to break the primary wave and form a spiral. A natural question is why this process depends on the average density, and the explanation is as follows. At sufficiently low average densities the passive spread

(a)



(b)

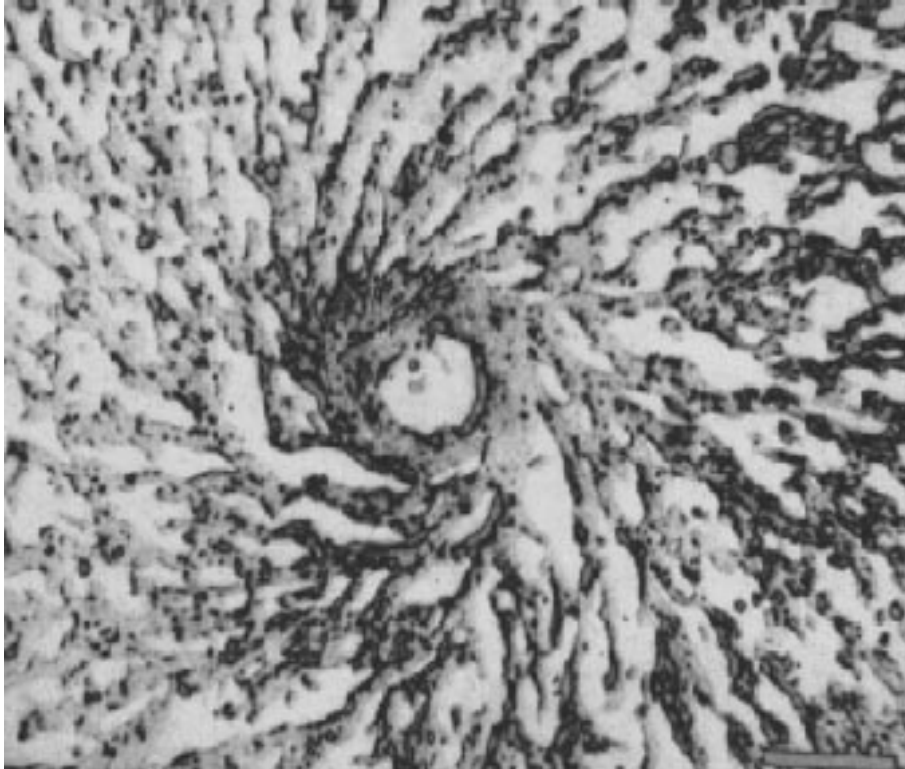


Figure 15. The experimentally observed aggregation centres: (a) normal (no caffeine added) aggregation, (b) aggregation in the presence of 2 mM caffeine. The scale bar in the lower right is 0.1 mm. (From Siegert & Weijer (1989), with permission.)

of cAMP never produces a superthreshold signal at the downstream side and the primary wave rejoins smoothly there, but at sufficiently high densities the passive spread can trigger a secondary wave. Long-range spread of cAMP through the low density region is possible because of the smaller affect of mPDE. Further work to determine whether this is the primary mechanism for break-up is in progress.

Once a wave is broken and a spiral is formed, it must be able to coexist with a pacemaker, at least for a period of time. It has been shown previously that a pacemaker can coexist with a spiral wave indefinitely in other excitable systems (Othmer & Tang 1993), but no theoretical explanation of this was given. It is known that for both pacemaker-initiated waves and spiral waves, their speed and period is such that the

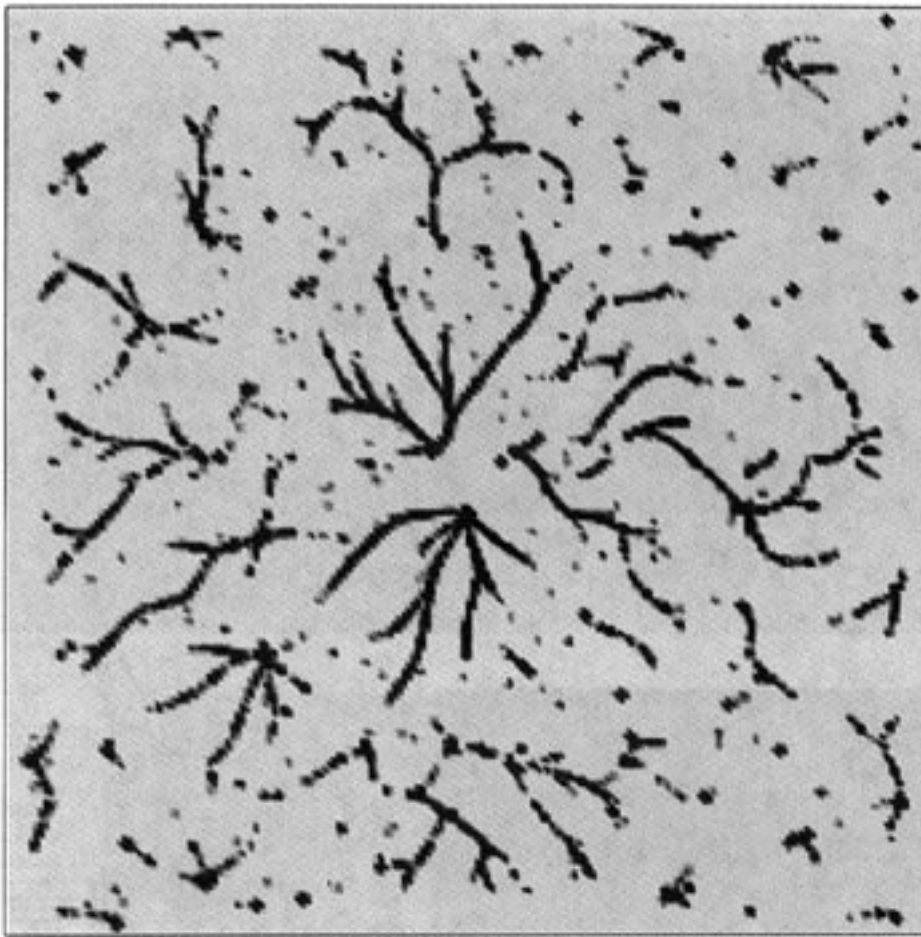


Figure 16. The aggregation pattern in a field of *wt/ACG* cells. The basal production of cAMP is increased by the constant amount 0.05 in each cell. Cells in the central disc are pacemakers as usual. The pattern is shown at 200 min and the  $u_2$  rules for movement are used. Black corresponds to densities of 1 or greater.

combination lies close to the dispersion curve for periodic travelling waves (figure 18*a*), and thus some insight into the effect of density on coexistence is obtained by calculating these dispersion curves for different densities. In order to do this, we must use a continuum rather than a discrete description of cell density. The dispersion curves are computed according to the procedure described in Monk & Othmer (1989*b*, 1990), and the results for four distinct densities are shown in figure 18*b*.

The range of periods of naturally occurring pacemakers is 3–10 min, and under the conditions used here the periods are in the range of 4–6 min. As a result, one can see from this figure that a high density field is more likely to propagate every wave initiated by a pacemaker, rather than gating the waves. Second, it is clear that higher density fields propagate stable waves over a much wider range of speed for pacemaker periods in the range used here, and thus coexistence between distinct types of waves is more likely at high densities. In particular, a spiral wave and an axisymmetric wave are more likely to coexist for some time in a high-density field. Such coexistence is essential to provide time for a spiral to develop in a field forced by a pacemaker. Once it is fully developed, it may or may not completely entrain the pacemaker.

The foregoing emphasizes the role of low-density regions in the breakup of waves, but high density regions can also have this effect. In other computational experiments we immobilized the pacemaker cells and allowed other cells to move as usual. This resulted in a small (*ca.* 0.3%) increase in density at the boundary between the pacemaker and the external field as mobile cells moved into the pacemaker region. We found that this small increase in density was sufficient to block propagation of the wave beyond the pacemaker region. In other cases heterogeneities can result in reflection rather than transmission of waves, thereby providing a third mechanism for wave block.

#### (e) *Simulations with many pacemakers*

In the computations described heretofore target patterns were generated by initially setting the parameters in a small disc of cells so as to make them oscillatory. Of course these cells were free to move about as the simulations progressed. However, DeYoung *et al.* (1988) have shown that single cells can act as pacemakers, and it is known experimentally that the fraction of cells that are pacemakers changes with the time since starvation. By randomly varying the value of  $\gamma_2$  for individual cells in a manner described in Appendix 3, we were able to test the effect

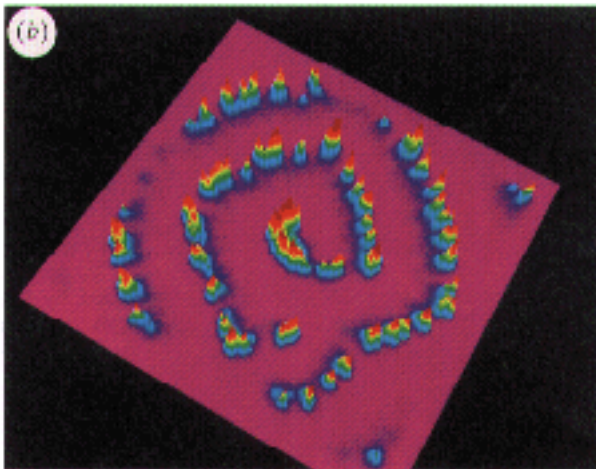
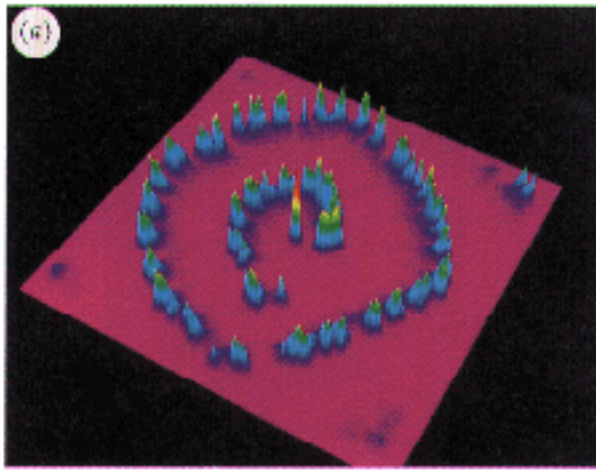


Figure 17. The cAMP wave for a simulation in which a spiral wave arises spontaneously in a field with a pacemaker at the centre. In (a)  $t = 95$  and the pacemaker fires before the spiral wave arrives. In (b)  $t = 110$  and the tip of the spiral coincides with the pacemaker. Concentrations greater than  $1 \mu\text{M}$  are shown in red and zero concentrations are represented by magenta.

of different percentages of pacemakers in an aggregation field. The results are shown in figure 19, where it is seen that the territory size of an aggregate depends strongly on the fraction of cells that are pacemakers. Simulations in which more than 0.1% of the cells have parameters in the oscillatory region form small aggregation territories, and can never develop territories of the 1 cm scale that is observed (McRobbie 1986). This agrees with the results of Raman *et al.* (1976), who found that the number of oscillatory cells is in the range 0.01–0.1% for the cell densities used in our simulations.

#### (f) *Direction selection*

Since the cAMP wave seen by a cell is very rough (cf. figure 10) and since there is undoubtedly noise in

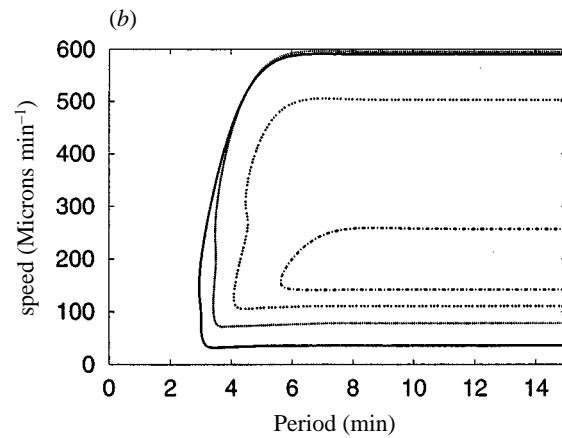
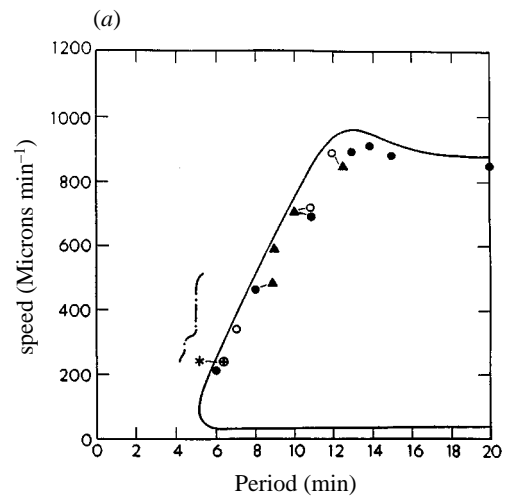


Figure 18. (a) The dispersion curve for the Monk–Othmer model of signal transduction in *Dd*. The symbols indicate various phase-locking ratios.  $\oplus$  denotes a computed spiral wave and  $*$  denotes a 1 to 1 response in a forced field. (From Monk & Othmer (1989b), with permission.) The short lines signify that two or more points are superimposed on the point closest to the curve. The broken line denotes the experimentally measured portion of the dispersion curve. (b) The dispersion curves for the present model using different uniform densities. The curves shown are for densities of 0.8 (solid line), 0.4, 0.2 and 0.1 (dash dot) left to right. The value of  $\gamma_2$  is 0.171 for all densities. The waves on the upper branch of each curve are stable and those on the lower branch are unstable.

the mechanism by which the direction of motion is selected, it is important to determine how reliably cells must orient themselves in the direction of the local cAMP gradient in order to aggregate successfully. To determine this, several experiments were conducted in which the true direction was replaced by one from a uniform distribution in a cone of specified angle whose centre line coincided with the direction of the cAMP gradient at that point. The results are shown in figure 22. An initially randomly distributed field can aggregate successfully when the cone angle is  $180^\circ$  (cf. figure 22b), but fails when the cone angle is more than  $250^\circ$ . Thus the system is quite robust in the sense that the cells need not detect the gradient

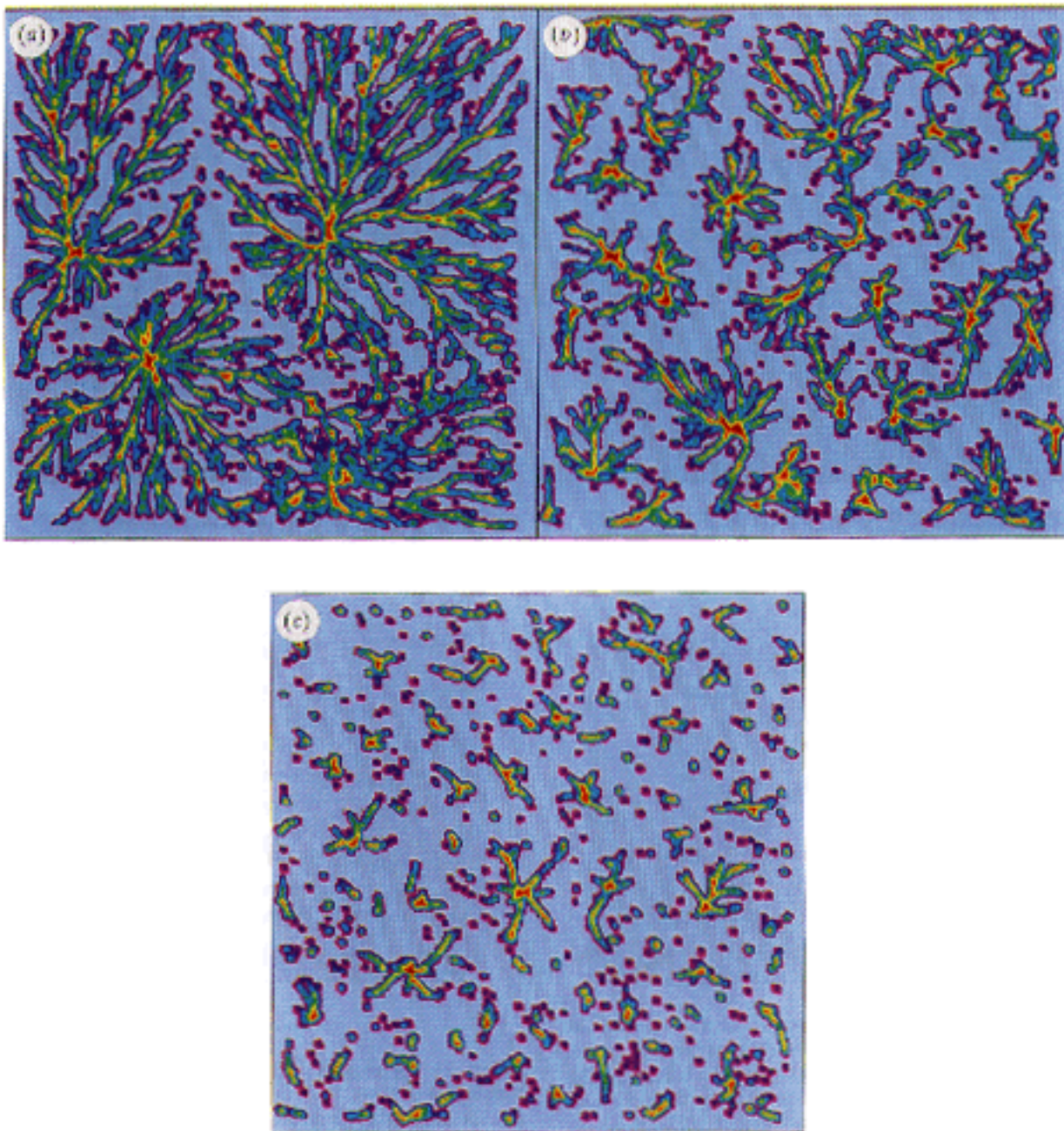


Figure 19. The aggregation patterns that result when 0.1% (a), 1% (b) and 10% (c) of the cells are allowed to be pacemakers. Cell densities of 1 and greater are shown in red.

precisely, but only have to orient themselves into the correct half-space in order to aggregate. Of course it takes longer to form a compact aggregate when the choice of direction is very sloppy, but it is possible.

#### 4. CONCLUSIONS

cAMP waves in an aggregation field are very irregular since they are the composite of waves initiated at each cell. Despite this, our simulations show that some biologically reasonable movement rules produce aggregation patterns very similar to those observed experimentally. Among the formal movement rules we tested, the  $u_2$  rules provide the most realistic description of individual cell movement, since they are based in part on what is known about the chemotac-

tic pathway in Dd. Our results also show that incorporating adaptation in the rules for individual cells prevents the cell from reversing course as the wave of cAMP passes (cf. figure 5), thereby resolving what has been called the ‘back-of-the-wave paradox’ (Soll *et al.* 1993).

Although it is found experimentally that cells are able to re-orient within 20 s in response to large stimuli, our results suggest that the cells do not re-orient this frequently under normal aggregation conditions. Persistence in the direction of movement can mitigate the effect of frequent sampling of the local gradient, but it seems that the best strategy is to choose a direction and continue this as long as the concentration is increasing, even if that increase has modified the local gradient sufficiently to warrant a re-

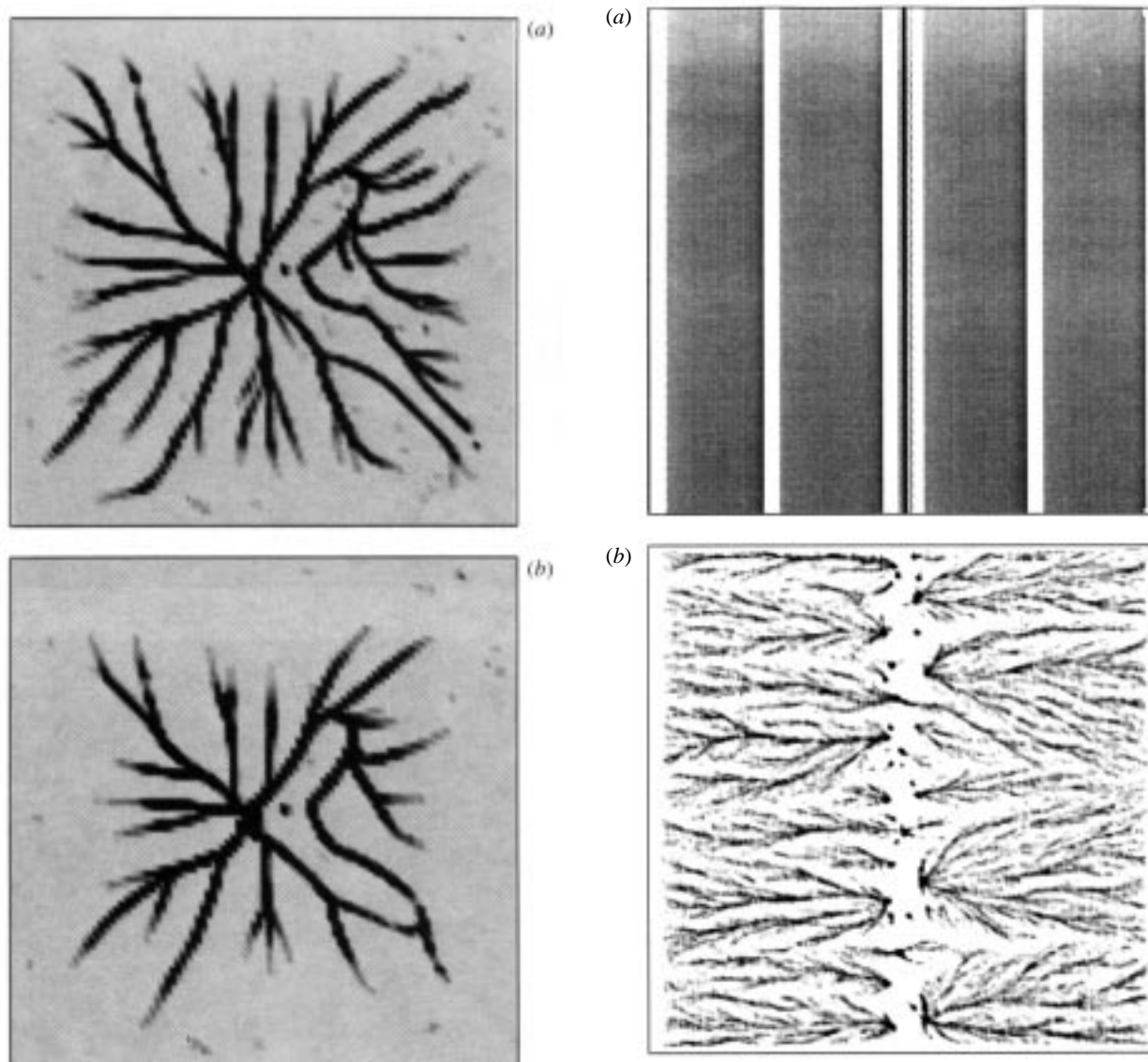


Figure 20. The aggregation patterns for the simulations on a cylinder. A vertical strip down the centre is the pace-making region. The average initial density is 0.2 and the results are shown at 70 min. The cells in these simulations are weighted by 4 with a total of 40 602 cells. In (a) the initial density is uniform, densities greater than 0.24 are shown in black, densities of less than 0.19 are shown in white, and all intermediate densities are shown in grey. In (b) the initial density is random, densities of 1 or more are shown in black, and intermediate densities are ramped between 0 (white) and 1. In (a) the cells are moving in the white strips halfway through the excitable region and stationary elsewhere, which reflects the outward propagating cAMP wave. These light bands are similar to those observed experimentally (Alcantara & Monk 1974).

orientation based on the current gradient. This is in agreement with the conclusions reached in Soll *et al.* (1993), where the authors state, 'We believe that cells realign polarity in the direction of the source sometime during this initial period, then move in a relatively blind fashion ...'.

A more accurate description of the mechanism that triggers cell movement is not possible until more of

Figure 21. Aggregation patterns from the same simulation as that shown in figure 9 after longer run times. In (a) the time is 400 min and in (b) the time is 800 min. Cell densities of 1 and greater are shown in black.

the biochemical machinery is understood. It seems likely that the choice of direction and subsequent movement is determined not by the local gradient, since cells cannot measure this accurately, but by a superthreshold signal at one point on the membrane which sets up an internal gradient that orients the assembly of the locomotory machinery. We are currently studying a two-cell model which will give us further insights into the orientation process. As we showed, the choice of direction can be quite sloppy and still lead to successful aggregation. Therefore whatever mechanism is used need not be terribly precise, which makes aggregation in this system very robust.

We also found that density has dramatic effects on the aggregation patterns. For example, we showed that spiral waves which are formed by breakup of a wave initiated from a pacemaker are less likely to

occur in fields with density less than *ca.* 0.2. Furthermore, random initial variations in the density play an important role in wave propagation at low densities, and density variations are one type of disturbance that can initiate streaming. Variations in the density have several consequences, including an effect on the speed of cAMP wave propagation (Monk & Othmer 1990) and the effect on the shape and amplitude of the cAMP wave. Other factors not directly related to the density, such as random differences in cell excitability, would also result in variations in the cAMP signal, which in turn can cause streaming. Our simulations using uniform initial densities lead us to conclude that a uniform spatial distribution of cells, all of which have identical characteristics, will aggregate without streaming. Thus we believe that streaming is the result of a finite-amplitude instability, and a heuristic argument supporting this contention was given earlier. If we are correct, it means that streaming cannot be understood from the linearized equations in the continuum description adopted by other authors (Levine & Reynolds 1991; Höfer *et al.* 1995). It might be argued that the linear instability grows very slowly, and that our computations do not show this on the timescale of normal aggregation, but if this is the case then such a mechanism cannot be relevant for explaining the observed streaming.

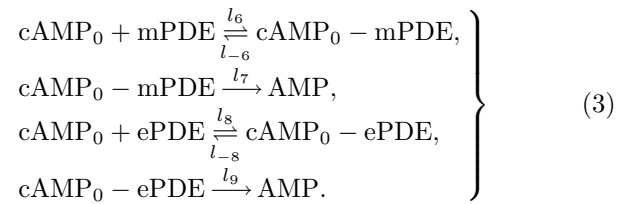
The simulations also support the idea that cell adhesion may be important in later stages of cell aggregation. Siu & Kamboj (1990) conducted experiments in which an antibody that prevents cell-cell adhesion was added to preparations. Some preparations would form streams, but none would progress beyond the mound stage. After 400 min in our simulations the cells are still moving towards the centre and have not formed a compact aggregate (cf. figure 21). The fact that the aggregate has not reached the mound morphology after this length of time could easily be explained by the absence of cell adhesion in our model. Cells adhering to each other could form a continuous moving stream by dragging each other along, thereby speeding the aggregation process up significantly. Moreover, in the absence of cell adhesion cells can cross cell streams and overshoot high density areas, which causes cells to zigzag and backtrack in an unrealistic manner.

Our model could be modified to simulate cell adhesion by imposing a correlation between the motion of cells that come into contact, perhaps by putting spring-like connections between cells. Such a modification is essential for describing late aggregation and the motion of the mound or slug.

This research was supported in part by NIH Grant GM #29123. The authors are indebted to Peter Monk, who was instrumental in the development of the algorithm used here. The visualization software SciAn used in producing the 2D images was provided by the Supercomputer Computations Research Institute and Florida State University.

## APPENDIX 1. CELL WEIGHTS

To describe the evolution of extracellular cAMP we modify the equations for the suspensions used in Tang & Othmer (1994). The modifications are only made in the equations for the extracellular quantities; the intracellular dynamics are the same. The extracellular reactions are



Here  $\text{cAMP}_0 - \text{mPDE}$  denotes the complex between cAMP and phosphodiesterase on the extracellular membrane, and  $\text{cAMP}_0 - \text{ePDE}$  the corresponding complex in the extracellular solution. The extracellular phosphodiesterase ePDE is assumed to be constant in space.

The modified differential equations are

$$\begin{aligned} V_0 \frac{\partial y_{14}}{\partial t} &= V_0 D \nabla^2 y_{14} + V_0 l_{-8} y_{16} - V_0 l_8 y_{14} z_9 \\ &+ \sum_{i=1}^N V_c \delta(x - x_i) \\ &\times \left( \frac{A_c}{V_c} dsr(y_{12}^i) + \frac{A_c}{V_c} l_{-6} y_{15}^i - \frac{A_c}{V_c} l_6 y_{14} z_8^i \right), \end{aligned} \quad (4)$$

$$\frac{dy_{15}^i}{dt} = -(l_{-6} + l_7) y_{15}^i + l_6 y_{14} z_8^i, \quad (5)$$

$$\frac{dy_{16}}{dt} = -(l_{-8} + l_9) y_{16} + cl_8 y_{14} z_9.$$

Here  $y_{14}$  stands for  $[\text{cAMP}_0]$ ,  $y_{15}^i$  for  $[\text{mPDE} - \text{cAMP}_0]$  for the  $i$ th cell,  $y_{16}$  for  $[\text{ePDE} - \text{cAMP}_0]$ ,  $z_8^i$  for free  $[\text{mPDE}]$  on the  $i$ th cell,  $z_9$  for the free  $[\text{ePDE}]$ ,  $A_c$  is the surface area of an individual cell,  $dsr$  is the dimensional secretion rate of cAMP, and  $N$  stands for the number of cells. The cells are assumed to have a volume of  $696.9 \mu\text{m}^3$  and a hemispherical shape, giving them a radius of  $\sqrt{2} \times 5.5 \mu\text{m}$ . They are assumed to be submerged in a fluid of depth  $\sqrt{2} \times 5.5 \mu\text{m}$ . Thus we calculate the surface area to be  $380 \mu\text{m}^2$ . In addition to the foregoing equations there are two other conservation equations, i.e.

$$y_{15}^i + z_8^i = [\text{mPDE}]_T^i, \quad y_{16} + z_9 = [\text{ePDE}]_T. \quad (6)$$

By scaling the new independent variables and introducing additional non-dimensional parameters, we obtain a non-dimensionalized system for the  $u_i$  and  $v_i$ . Most of the equations are the same as in Tang & Othmer (1994). The newly introduced dimensionless parameters and rapidly varying quantities are listed in table 2. We scale  $y_{14}$  as follows:  $w_5 = y_{14}/[\text{IPDE}]_T$ . The differential equations for the rapidly varying quantities are

$$\left. \begin{aligned} \epsilon_7 \frac{dv_7^i}{d\tau} &= w_5 - v_7^i - \frac{1}{\gamma_6} w_5 v_7^i, \\ \epsilon_8 \frac{dv_8}{d\tau} &= w_5 - v_8 - \frac{1}{\gamma_8} w_5 v_8. \end{aligned} \right\} \quad (7)$$

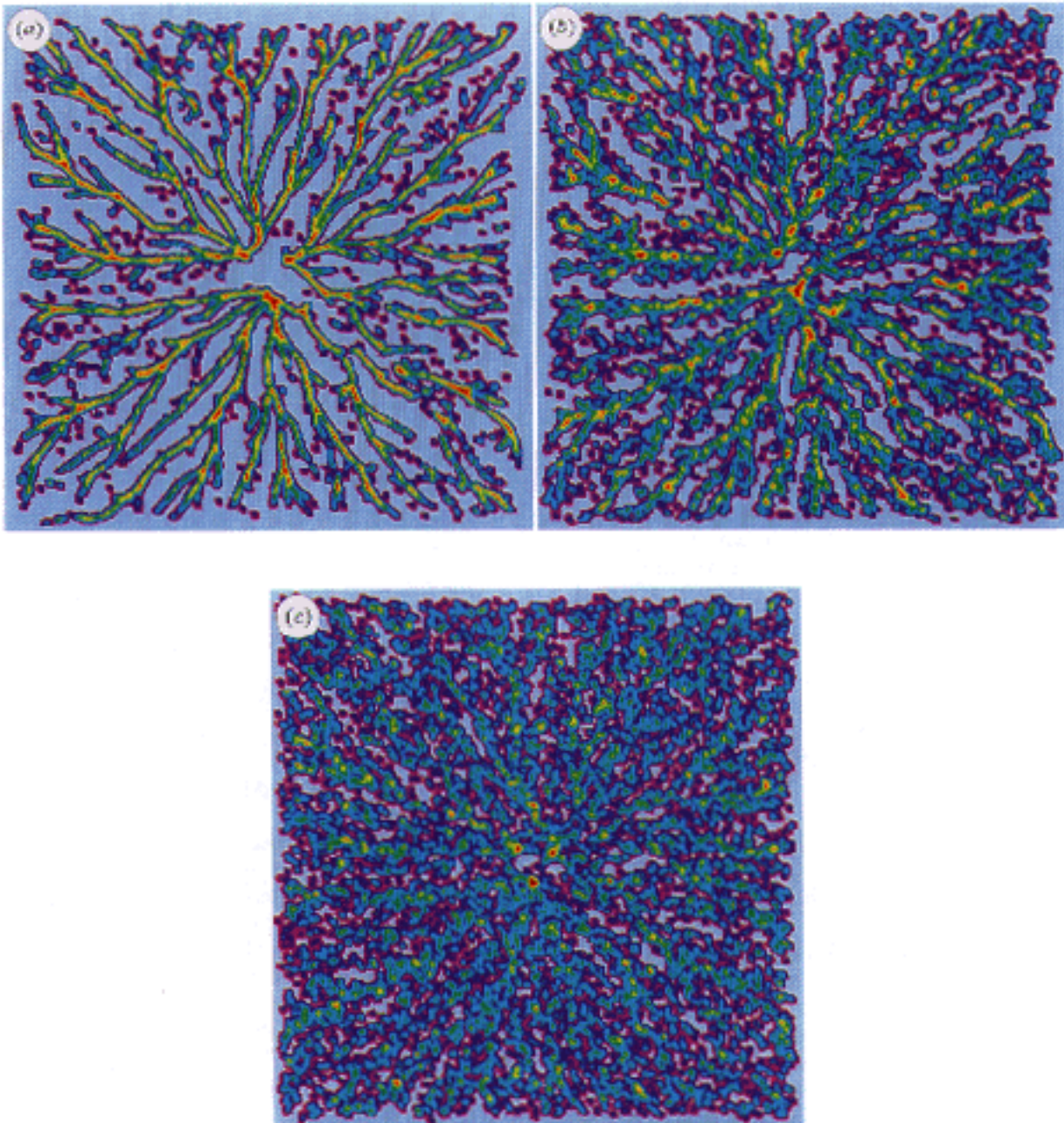


Figure 22. Aggregation patterns for simulations which tested the sensitivity to direction selection. In (a) the cells move in the direction of the gradient with certainty, in (b) the direction of motion is varied randomly within a cone centred at the gradient with an angle of  $180^\circ$ , and in (c) the cone angle is  $250^\circ$ . The simulations use the standard parameters and a random initial cell distribution. The results in each case are shown at 150 min. Cell densities of 1 and greater are shown in red.

We set the time derivatives for these variables equal to zero, solve the resulting system, and use the results in the equations for the slowly varying variables. The result is that the new equations are equations (1) and (2) in § 2.

## APPENDIX 2. THE NUMERICAL METHODS AND THEIR IMPLEMENTATION

The equations to be solved are of the form

$$\frac{\partial u}{\partial t} = D\Delta u + \sum_{i=1}^N F_i(u, \mathbf{v}_i, x, y) + F(u), \quad (8)$$

$$\frac{d\mathbf{v}_i}{dt} = \mathbf{G}_i(\mathbf{v}_i, u), \quad (9)$$

where  $u$  stands for the concentration of external cAMP,  $F(u)$  represents the degradation of cAMP by extracellular PDE,  $F_i(u, \mathbf{v}_i, x, y)$  are terms that represent a cell's production of cAMP and degradation of cAMP via membrane bound PDE,  $\mathbf{v}_i$  are vectors which represent the intracellular variables,  $\mathbf{G}_i$  are vectors representing the intracellular dynamics with  $i$  ranging from 1 to  $N$  where  $N$  is the number of cells.

The numerical method we developed to solve this system is similar to a particle-in-cell method (O'Rourke & Brackbill 1993). Equation (8) is

Table 2. Additional dimensionless variables and parameters

parameters	parameters	variables
$\alpha_0 = \frac{k_1[\text{iPDE}]_T}{k_5}$	$\gamma_8 = \frac{l_{-8} + l_9}{l_8[\text{iPDE}]_T}$	$v_7^i = \frac{(l_{-6} + l_7)y_{15}^i}{l_6[\text{iPDE}]_T[\text{mPDE}]_T}$
$\beta_0 = \frac{h_1[\text{iPDE}]_T}{k_5}$	$\gamma_9 = \frac{l_9[\text{ePDE}]_T}{k_5[\text{iPDE}]_T}$	$v_8 = \frac{(l_{-8} + l_9)y_{16}}{l_8[\text{iPDE}]_T[\text{ePDE}]_T}$
$\gamma_6 = \frac{l_{-6} + l_7}{l_6[\text{iPDE}]_T}$	$\epsilon_7 = \frac{k_5}{l_{-6} + l_7}$	
$\gamma_7 = \frac{l_7[\text{mPDE}]_T A_c}{k_5[\text{iPDE}]_T V_c}$	$\epsilon_8 = \frac{k_5}{l_{-8} + l_9}$	

solved using an alternating-direction implicit method (Peaceman & Rachford 1955) with the intracellular variables lagged in time, and then the equations for the intracellular variables are advanced with  $u$  time-lagged. Since the cells are not restricted to lie at grid points we must transfer cAMP from grid to cell and vice versa during the time-stepping. Before we give the discretized equations we define a tensor product interpolating operator (Alfeld 1989):

$$I[F_i] = \begin{cases} \frac{(x_{w+1} - x^i)(y_{s+1} - y^i)}{h_x^2 h_y^2} F_{\text{at}}(x_w, y_s), \\ \frac{(x^i - x_w)(y_{s+1} - y^i)}{h_x^2 h_y^2} F_i, \text{ at } (x_{w+1}, y_s), \\ \frac{(x_{w+1} - x^i)(y^i - y_s)}{h_x^2 h_y^2} F_i, \text{ at } (x_w, y_{s+1}), \\ \frac{(x^i - x_w)(y^i - y_s)}{h_x^2 h_y^2} F_i, \text{ at } (x_{w+1}, y_{s+1}), \\ 0, \text{ otherwise.} \end{cases} \quad (10)$$

$I$  interpolates  $u$  from the cells to the grid where  $(x^i, y^i)$  is the position of the  $i$ th cell,  $(x_w, y_s)$  is the nearest grid point to the cell in the southwest direction and  $h_x$  and  $h_y$  are the distances between grid points in the  $x$  and  $y$  directions respectively. This tensor product interpolation gives a unique, continuous, bivariate, piecewise linear polynomial which has a specified maximum at the cell location, is always non-negative (we define it to be zero where it is not positive), whose integral is equal to the value  $F_i$  (conserves mass) and given any slice in the  $x$  or  $y$  direction the function decreases from the maximum at the same rate. These are all characteristics of the heat equation. In fact, the sequence of interpolants  $I_n[1]$  where  $h_x = h_y = 1/n$  is a delta sequence as it should be. Recall that the  $F_i$ 's are point sources or sinks for the diffusing chemical, so as  $h_x = h_y \rightarrow 0$  the interpolant should approximate the Dirac distribution. Now define

$$T(u, x^i, y^i) = \sum_{n=-2}^2 \left( \sum_{m=-2}^2 u_{j-m, k-n} \ell_{j-m}(x^i) \right) \ell_{k-n}(y^i), \quad (11)$$

where

$$\ell_j(x) = \frac{(x - x_{j-2})(x - x_{j-1})(x - x_{j+1})(x - x_{j+2})}{(x_j - x_{j-2})(x_j - x_{j-1})(x_j - x_{j+1})(x_j - x_{j+2})}. \quad (12)$$

$T$  interpolates  $u$  from the grid to the cell. Since the grid is a regular rectangular grid,  $T$  is a tensor product interpolant using quartic Lagrangian interpolation in each direction (Ralston & Rabinowitz 1978). In equation (11)  $u_{j,k}$  is the value of  $u$  at the grid point  $(x_j, y_k)$  which is the closest grid point to  $(x^i, y^i)$ . The error introduced by  $T$  is  $O(h_x^q h_y^p) \propto h_x^q h_y^p$  where  $q + p = 5$ . (For our computations  $h_x = h_y$  and so the error is  $O(h_x^5)$ .) Next we define a standard fourth-order difference approximation to the  $x$  and  $y$  components of the Laplacian:

$$\left. \begin{aligned} \delta_x^* f &= \frac{1}{12} [-f(x_0 - 2h_x, y_0) + 16f(x_0 - h_x, y_0) - 30f(x_0, y_0) + 16f(x_0 + h_x, y_0) - f(x_0 + 2h_x, y_0)], \\ \delta_y^* f &= \frac{1}{12} [-f(x_0, y_0 - 2h_y) + 16f(x_0, y_0 - h_y) - 30f(x_0, y_0) + 16f(x_0, y_0 + h_y) - f(x_0, y_0 + 2h_y)]. \end{aligned} \right\} \quad (13)$$

The cells are excluded from a strip of width one grid cell at the boundary, and we impose homogeneous Dirichlet conditions on cAMP at the boundary. Since the waves propagate outward and the cells move away from the boundary these are appropriate. In addition we impose a symmetry condition at the boundary which forces the derivatives to vanish as well. This is done to simplify the use of higher-order approximations to the derivatives and does not affect the accuracy of the results.

The scheme can now be described by the following discretized equations:

$$\begin{aligned} u_{\ell,m}^{n+1/2} - u_{\ell,m}^n &= \frac{Dk}{2} \left( \frac{\delta_x^* u_{\ell,m}^{n+1/2}}{h_x^2} + \frac{\delta_y^* u_{\ell,m}^n}{h_y^2} \right) \\ &+ \frac{k}{2} \left[ F(u_{\ell,m}^n) + \sum_{i=1}^N I_{\ell,m}[F_i(T(u^n, x^i, y^i), \mathbf{v}_i^n)] \right], \end{aligned} \quad (14)$$

$$u_{\ell,m}^{n+1} - u_{\ell,m}^{n+1/2} = \frac{Dk}{2} \left( \frac{\delta_x^* u_{\ell,m}^{n+1/2}}{h_x^2} + \frac{\delta_y^* u_{\ell,m}^{n+1/2}}{h_y^2} \right) + \frac{k}{2} \left[ F(u_{\ell,m}^{n+1}) + \sum_{i=1}^N I_{\ell,m} [F_i(T(u^n, x^i, y^i), \mathbf{v}_i^n)] \right]. \quad (15)$$

Here  $k$  is the time step,

$$u_{\ell,m}^n = u((\ell - 1)h_x, (m - 1)h_y, nk),$$

$$I_{\ell,m} = I[F_i]((\ell - 1)h_x, (m - 1)h_y)$$

and  $\mathbf{v}_i^n = \mathbf{v}_i(nk)$ . The system of nonlinear algebraic equations is solved using the software package NK-SOLV (Brown & Saad 1987).

Next the ordinary differential equations (8) are solved. They are discretized using the trapezoidal rule and the system is solved using Newton iterations. The discretized equations are

$$\mathbf{v}_i^{n+1} - \mathbf{v}_i^n = \frac{1}{2}k[\mathbf{G}(\mathbf{v}_i^{n+1}, T(u^{n+1}, x^i, y^i)) + \mathbf{G}(\mathbf{v}_i^n, T(u^{n+1}, x^i, y^i))].$$

At a density of  $6.4 \times 10^5$  cells  $\text{cm}^{-2}$  there are 16 cells per grid cell, and these are replaced by one equivalent cell. In the numerical scheme we interpolate the concentration from the cells to the grid. Thus if the cells are all in one grid square the interpolation to the grid should make both cases (weighted or evenly separated) almost indistinguishable. The interpolation from the grid to the cells will maintain some distinction between the two cases. If we choose the cell shape to be a half cylinder (without ends) rather than a hemisphere we would need to multiply each cell by  $\frac{2}{3}$  in order to keep the appropriate concentrations per cell. This would make the cell weighting about 10 for each cell. One can see that the matter of cell weighting is somewhat ambiguous even though the cAMP concentration per cell is maintained to agree with experimental data.

### APPENDIX 3. RANDOM VARIABLES

For the case of cells with different  $\gamma_2$  values,  $\gamma_2$  can take on 31 evenly spaced values ranging from 0.1 to 0.4. The oscillatory range is from 0.18 to 0.4. The probability mass functions used are

$$p(x_i) = \begin{cases} 0.04, & \text{for } x_i \in [0.1, 0.14], \\ 0.099, & \text{for } x_i = 0.15, \\ 0.35, & \text{for } x_i \in [0.16, 0.17], \\ 0.000\,043, & \text{for } x_i \in [0.18, 0.4], \end{cases}$$

giving 0.1% in the oscillatory region,

$$p(x_i) = \begin{cases} 0.04, & \text{for } x_i \in [0.1, 0.14], \\ 0.09, & \text{for } x_i = 0.15, \\ 0.35, & \text{for } x_i \in [0.16, 0.17], \\ 0.000\,43, & \text{for } x_i \in [0.18, 0.4], \end{cases}$$

giving 1% in the oscillatory region and

$$p(x_i) = \begin{cases} 0.02, & \text{for } x_i \in [0.1, 0.14], \\ 0.1, & \text{for } x_i = 0.15, \\ 0.35, & \text{for } x_i \in [0.16, 0.17], \\ 0.0043, & \text{for } x_i \in [0.18, 0.4], \end{cases}$$

giving 10% in the oscillatory region.

### REFERENCES

- Alcantara, F. & Monk, M. 1974 Signal propagation during aggregation in the slime mold *Dictyostelium discoideum*. *J. Gen. Microbiol.* **85**, 321–334.
- Alfeld, P. 1989 Scattered data interpolation in three or more variables. *Mathematical methods in computer aided geometric design* (ed. T. Lyche & L. Schumaker), pp. 1–33. Boston: Academic Press.
- Bonner, J. T. 1982 Comparative biology of cellular slime molds. *The development of Dictyostelium discoideum* (ed. W. F. Loomis), pp. 1–33. Academic Press.
- Brown, P. N. & Saad, Y. 1987 Hybrid Krylov methods for nonlinear systems of equations. Llnl Rep. ucr1-97645.
- Claviez, M., Brink, M. & Gerisch, G. 1986 Cytoskeletons from a mutant of *Dictyostelium discoideum* with flattened cells. *J. Cell Sci.* **86**, 69–82.
- Dallon, J. & Othmer, H. G. 1997 A continuum analysis of the chemotactic signal seen by aggregation-competent slime mold cells. (In preparation.)
- Devreotes, P. N. 1982 Chemotaxis. In *The development of Dictyostelium discoideum*, pp. 117–168. New York: Academic Press.
- DeYoung, G., Monk, P. B. & Othmer, H. G. 1988 Pacemakers in aggregation fields of *Dictyostelium discoideum*. Does a single cell suffice? *J. Math. Biol.* **26**, 486–517.
- Durston, A. J. 1974 Pacemaker activity during aggregation in *Dictyostelium discoideum*. *Dev. Biol.* **37**, 225–235.
- Fisher, P. R. 1990 Pseudopodium activation and inhibition signals in chemotaxis by *Dictyostelium discoideum* amoebae. *Cell Biol.* **1**, 87–97.
- Futrelle, R., Traut, J. & McKee, W. G. 1982 Cell behavior in *Dictyostelium discoideum*: preaggregation response to localized cyclic AMP pulses. *J. Cell. Biol.* **92**, 807–821.
- Gingle, A. R. & Robertson, A. 1976 The development of the relaying competence in *Dictyostelium discoideum*. *J. Cell Sci.* **20**, 21–27.
- Höfer, T., Sherratt, J. A. & Maini, P. K. 1995 *Dictyostelium discoideum*: cellular self-organization in an excitable biological medium. *Proc. R. Soc. Lond. B* **259**, 249–257.
- Kuwayama, H., Ishida, S. & Van Haastert, P. J. M. 1993 Non-chemotactic *Dictyostelium discoideum* mutants with altered cGMP signal transduction. *J. Cell Biol.* **123**(6), 1453–1462.
- Lee, K. J., Cox, E. C. & Goldstein, R. E. 1996 *Competing patterns of signalling activity in Dictyostelium discoideum*. Preprint.
- Levine, H. & Reynolds, W. 1991 Streaming instability of aggregating slime mold amoebae. *Phys. Rev. Lett.* **70**, 2400–2403.
- Lilly, P. J. & Devreotes, P. N. 1995 Chemoattractant and GTP $\gamma$ S-mediated stimulation of adenyl cyclase in *Dictyostelium* requires translocation of CRAC to membranes. *J. Cell Biol.* **129**, 1659–1653.
- Loomis, W. F. 1975 *Dictyostelium discoideum: a developmental system*. Academic Press.
- MacKay, S. 1978 Computer simulation of aggregation in *Dictyostelium discoideum*. *J. Cell. Sci.* **33**, 1–16.
- Martiel, J. L. & Goldbeter, A. 1984 Oscillations and relay of cAMP signals in *Dictyostelium discoideum*: analysis of a model based on the modification of the cAMP receptors. *C.R. Acad. Sci. Paris III* **298**, 549–552.
- McRobbie, S. J. 1986 Chemotaxis and cell motility in the cellular slime molds. *Crit. Rev. Microbiol.* **13**, 335–375.

- Monk, P. B. & Othmer, H. G. 1989a Cyclic AMP oscillations in suspensions of *Dictyostelium discoideum*. *Phil. Trans. R. Soc. Lond. B* **323**, 185–224.
- Monk, P. B. & Othmer, H. G. 1989b Relay, oscillations and wave propagation in a model of *Dictyostelium discoideum*. In *Lectures on mathematics in life sciences* (ed. H. G. Othmer), pp. 87–120. Providence, RI: AMS.
- Monk, P. B. & Othmer, H. G. 1990 Wave propagation in aggregation fields of the cellular slime mold *Dictyostelium discoideum*. *Proc. R. Soc. Lond. B* **240**, 555–589.
- Newell, P. C., Europe-Finner, G. N., Liu, G., Gammon, B. & Wood, C. A. 1990 Chemotaxis of *Dictyostelium discoideum*: the signal transduction pathway to actin and myosin. In *Biology of the chemotactic response* (ed. J. P. Armitage & J. M. Lackie), pp. 241–272. Cambridge University Press.
- O'Rourke, P. J. & Brackbill, J. U. 1993 On particle-grid interpolation and calculating chemistry in particle-in-cell methods. *J. Comp. Phys.* **109**, 37–52.
- Othmer, H. G. 1997 Adaptation in models of cellular movement. (In preparation.)
- Othmer, H. G. & Tang, Y. 1993 Oscillations and waves in a model of IP<sub>3</sub>-controlled calcium dynamics. In *Experimental and theoretical advances in pattern formation* (ed. H. G. Othmer, P. K. Maini & J. D. Murray), pp. 277–313. Plenum Press.
- Parnas, H. & Segel, L. A. 1977 Computer evidence concerning the chemotactic signal in *Dictyostelium discoideum*. *J. Cell Sci.* **25**, 191–204.
- Peaceman, D. W. & Rachford Jr, H. H. 1955 The numerical solution of parabolic and elliptic differential equations. *J. Soc. Indust. Appl. Math* **3**, 28–41.
- Pitt, G. S., Brandt, R., Lin, K. C., Devreotes, P. N. & Schaap, P. 1993 Extracellular cAMP is sufficient to restore developmental gene expression and morphogenesis in *Dictyostelium* cells lacking the aggregation adenylyl cyclase (ACA). *Genes Devel.* **7**, 2172–2180.
- Ralston, A. & Rabinowitz, P. 1978 *A first course in numerical analysis*. New York: McGraw-Hill.
- Raman, R. K., Hashimoto, Y., Cohen, M. H. & Robertson, A. 1976 Differentiation for aggregation in the cellular slime molds: the emergence of autonomously signalling cells in *Dictyostelium discoideum*. *J. Cell. Sci.* **21**, 243–259.
- Raper, K. B. 1984 *The Dictyostelids*. Princeton University Press.
- Ross, F. M. & Newell, P. C. 1981 Streamers: chemotactic mutants of *Dictyostelium discoideum* with altered cyclic GMP metabolism. *J. Gen. Microbiol.* **127**, 339–350.
- Ross, S. 1994 *A first course in probability*, 4th edn. Macmillan College Publishing.
- Schaap, P., Tang, Y. & Othmer, H. G. 1997 A model for pattern formation in *Dictyostelium discoideum*. *Differentiation*. (In the press.)
- Siebert, F. & Weijer, C. 1989 Digital image processing of optical density wave propagation in *Dictyostelium discoideum* and analysis of the effects of caffeine and ammonia. *J. Cell Sci.* **93**, 325–335.
- Siu, C.-H. & Kamboj, R. K. 1990 Cell-cell adhesion and morphogenesis in *Dictyostelium discoideum*. *Dev. Gen.* **11**, 277–387.
- Snaar-Jagalska, E. & Van Haastert, P. J. M. 1990 Pertussis toxin inhibits cAMP-induced desensitization of adenylyl cyclase in *Dictyostelium discoideum*. *Molec. Cell. Biochem.* **92**, 177–189.
- Soll, D. R., Wessels, D. & Sylwester, A. 1993 The motile behavior of amoebae in the aggregation wave in *Dictyostelium discoideum*. In *Experimental and theoretical advances in biological pattern formation* (ed. H. G. Othmer, P. K. Maini & J. D. Murray). London: Plenum.
- Tang, Y. & Othmer, H. G. 1994 A G-protein-based model of adaptation in *Dictyostelium discoideum*. *Math. Biosci.* **120**, 25–76.
- Tang, Y. & Othmer, H. G. 1995 Excitation, oscillations and wave propagation in a G-protein based model of signal transduction in *Dictyostelium discoideum*. *Phil. Trans. R. Soc. Lond. B* **349**, 179–195.
- Theibert, A. & Devreotes, P. N. 1986 Surface receptor-mediated activation of adenylyl cyclase in *Dictyostelium discoideum*. *J. Biol. Chem.* **261**, 15121–15125.
- Tomchik, K. J. & Devreotes, P. N. 1981 Adenosine 3', 5'-monophosphate waves in *Dictyostelium discoideum*: a demonstration by isotope dilution-fluorography. *Science* **212**, 443–446.
- Tyson, J. J., Alexander, K. A., Manoranjan, V. S. & Murray, J. D. 1989 Spiral waves of cyclic AMP in a model of slime mold aggregation. *Physica D* **34**, 193–207.
- Valkema, R. & Van Haastert, P. J. M. 1994 A model for cAMP-mediated cGMP response in *Dictyostelium discoideum*. *Molec. Biol. Cell* **5**, 575–585.
- Varnum, B., Edwards, K. B. & Soll, D. R. 1985 *Dictyostelium* amoebae alter motility differently in response to increasing versus decreasing temporal gradients of cAMP. *J. Cell Biol.* **101**, 1–5.
- Varnum-Finney, B. J., Voss, E. & Soll, D. R. 1987 Frequency and orientation of pseudopod formation of *Dictyostelium discoideum* amoebae chemotaxing in a spatial gradient: further evidence for a temporal mechanism. *J. Cell Motil. Cytoskeleton* **8**, 18–26.
- Vasiev, B. N., Hogeweg, P. & Panfilov, A. V. 1994 Simulation of *Dictyostelium discoideum* aggregation via reaction-diffusion model. *Phys. Rev. Lett.* **73**, 3173–3176.
- Vasieva, O. O., Vasiev, B. N., Karpov, V. A. & Zaikin, A. N. 1994 A model of *Dictyostelium* aggregation. *J. Theor. Biol.* **171**, 361–367.
- Wessels, D., Soll, D. R., Knecht, D., Loomis, W. F., DeLozanne, A. & Spudich, J. A. 1988 Cell motility and chemotaxis in *Dictyostelium* amoebae lacking myosin heavy chain. *Dev. Biol.* **128**, 164–177.

Received 19 February 1996; accepted 2 May 1996